

Gravitino Thermal Production, Dark Matter, and Reheating of the Universe

Helmut Eberl ^a, Ioannis D. Gialamas ^b, Vassilis C. Spanos ^{c,d}

^a*Institut für Hochenergiephysik der Österreichischen Akademie der Wissenschaften, A-1050 Vienna, Austria*

^b*Laboratory of High Energy and Computational Physics, National Institute of Chemical Physics and Biophysics, Rävala pst. 10, Tallinn, 10143, Estonia*

^c*William I. Fine Theoretical Physics Institute, School of Physics and Astronomy, University of Minnesota, 116 Church Street S.E., Minneapolis, MN 55455, USA*

^d*Section of Nuclear and Particle Physics, Department of Physics, National and Kapodistrian University of Athens, GR-15784 Athens, Greece*

E-mail: helmut.eberl@oeaw.ac.at, ioannis.gialamas@kbfj.ee,
vspanos@phys.uoa.gr

Abstract. We present a full one-loop calculation of the gravitino thermal production rate, beyond the so-called hard thermal loop approximation, using the corresponding thermal spectral functions in numerical form on both sides of the light cone. This framework requires a full numerical evaluation. We interpret our results within the framework of a general supergravity-based model, remaining agnostic about the specifics of supersymmetry breaking. In this context, assuming that gravitinos constitute the entirety of the dark matter in the Universe imposes strict constraints on the reheating temperature. For example, with a gluino mass at the current LHC limit, a maximum reheating temperature of $T_{\text{reh}} \simeq 10^9$ GeV is compatible with a gravitino mass of $m_{3/2} \simeq 1$ TeV. Additionally, with a reheating temperature an order of magnitude lower at $T_{\text{reh}} \simeq 10^8$ GeV, the common gaugino mass $M_{1/2}$ can range from 2 to 4 TeV within the same gravitino mass range. For much higher values of $M_{1/2}$, which are favored by current accelerator and cosmological data in the context of supersymmetric models, such as $M_{1/2} = 10$ TeV, and for $m_{3/2} \simeq 1$ TeV the reheating temperature compatible with the gravitino dark matter scenario is 10^7 GeV. If other dark matter particles are considered, the reheating temperature could be much lower.

preprint number: FTPI-MINN-24/20

Contents

1	Introduction	2
2	General framework	5
3	The $2 \rightarrow 2$ processes and their subtracted part	6
3.1	The squared amplitudes	7
3.2	The subtracted rate	8
3.3	Top Yukawa contribution to the thermal rate	10
3.4	Thermally corrected gravitino self-energy	12
4	The total gravitino thermal production rate	18
5	Gravitino abundance, DM and reheating temperature	19
6	Conclusions	24
A	Amplitudes	26
A.1	Couplings	26
A.2	Kinematics	27
A.3	Involved interactions	28
A.4	Goldstino production	32
A.4.1	The derivative approach	32
A.4.2	The non-derivative approach	33
B	Thermal spectral functions	35
B.1	Vector-boson self-energy	35
B.2	Fermion self-energy	37
B.3	Dispersion relations	38
B.3.1	Vector-bosons	38
B.3.2	Fermions	38
C	Calculation of the collision term	39

1 Introduction

Although supersymmetry (SUSY) and its local extension, supergravity (SUGRA), lack experimental verification, they still remain a promising comprehensive framework for new physics beyond the standard model (SM) of particle physics. In the context of these models, two particles can play the role of the dark matter (DM) in the Universe: the lightest neutralino, an admixture of neutral gauginos and higgsinos, and the gravitino. The latter scenario is favoured by the negative direct DM detection results, till now. The neutralino abundance has been calculated precisely [1–3], without any important approximation. On the other hand, the gravitino’s abundance calculation is quite different, as it interacts purely gravitationally with the plasma. Therefore, the gravitino is the prototype of a freeze-in DM particle and it is produced mainly thermally.

Since, the dominant production of gravitinos takes place at a quite high temperature, they are assumed to be massless. In this regime the so-called non-derivative approach [4], involving only the spin 1/2 goldstino components was used. In this effective theory approach, some production amplitudes exhibit infrared (IR) divergences [5, 6]. Therefore, they were regularised either using a finite thermal gaugino mass or an angular cutoff, in the phase-space integration [7, 8]. In [9] the basic $2 \rightarrow 2$ gravitino production processes had been classified and calculated. This calculation was revised in [10, 11]. Furthermore, in [12] the authors applied the Braaten-Pisarski-Yuan (BPY) method [13–15] for the calculation of the gravitino production rate, in the HTL limit. In [5] the IR singularities were regularized as described above using, finite thermal masses for gauginos. Moreover, in [6, 16] the BPY method was employed, taking in addition into account the contribution of the spin 3/2 gravitino components. Since this contribution is of the order $M_N^2/m_{3/2}^2$, where $M_{1,2,3}$, and $m_{3/2}$ are the gauginos and gravitino mass respectively, their result is valid also in the finite gravitino mass regime.

The calculation method developed even more in [17]. The authors argued that the basic condition in order to apply the BPY prescription, that is $g \ll 1$, where g is the gauge coupling constant, is not satisfied for every temperature, especially if g is the strong coupling constant. For this reason, the full one-loop thermal gravitino self-energy must be calculated numerically beyond the hard thermal loop (HTL) approximation. The main idea is that the one-loop gravitino selfenergy through the optical theorem contains all the $1 \rightarrow 2$ processes and the majority of the $2 \rightarrow 2$ (refer also to [18, 19] for three-body gravitino decays in the MSSM). The $2 \rightarrow 2$ processes that are not related to the selfenergy is the so-called subtracted part and must be calculated separately. Interestingly enough, this part is free of IR singularities [17].

Recently, we have revisited this calculation [20]. We corrected errors of the previous analysis and we presented a new numerical result that was differed from that in [17] by almost 10%. In this paper we provide all the analytical tools and results that are required for the calculation of the gravitino selfenergy. Moreover, in our numerical calculation we use the full one-loop numerical result for the spectral functions. This way one can calculate the gravitino selfenergy without any numerical approximation in the whole frequency-momentum plane, that is both inside and outside of the light

cone. This more detailed numerical treatment yields an updated result for the thermal gravitino production rate, which is approximately 40% lower than that reported in [20]. This reduction diminishes with increasing temperatures, reaching around 20% at $T \sim 10^8$ GeV, and disappears entirely at $T \sim 10^{16}$ GeV.

Since the gravitino abundance is related to the maximum reheating temperature, T_{reh} , the reduced production rate allows for higher T_{reh} for a given $m_{3/2}$, as required for successful thermal leptogenesis [21–28]. The cosmological consequences of this will be discussed in details below.

Depending on the cosmological period, gravitinos may be produced in various ways. (a) They can be produced through the inflaton decays [29–39], (b) thermally, as the Universe cools down from the T_{reh} until now [5–12, 16, 17, 20, 36, 40–44] and (c) through the decays of unstable particles [45–48] around the big bang nucleosynthesis (BBN). In the context of the gauge mediated supersymmetry breaking scenario, a different production mechanism is used [49–53]¹. Recently, an alternative scenario has gained attention, focusing on the so-called “catastrophic” non-thermal production of slow gravitinos [98–103]. Additionally, studies on gravitino and swampland conjectures have appeared in [104, 105], although the realization of inflation in this scenario appears to be quite challenging. More comprehensive studies on the production of spin-3/2 particles can be found in [39, 106–110], while constraints on their mass based on the recent $(g - 2)_\mu$ measurement are discussed in [111].

In our analysis, we will remain agnostic about the specifics of SUSY breaking and, consequently, about which particle plays the role of DM. In SUGRA-based models, there are numerous candidates² for this role: neutral gauginos or specific mixtures of them (such as the neutralino), sneutrinos, axions, axinos, and, last but not least, the gravitino. In popular and well-studied models within this context, such as the minimal mSUGRA and the Constrained Minimal Supersymmetric Standard Model (CMSSM), the natural DM particle, beyond the gravitino, is the neutralino.

In the CMSSM, where $m_{3/2}$ is not related to the other soft SUSY-breaking masses, the lightest supersymmetric particle (LSP) and DM candidate can be either the gravitino or the neutralino. It is important to note that there will be thermal production of gravitinos in either case. If the gravitino is the LSP and the DM particle, there are at least two additional production mechanisms for gravitinos, beyond thermal production, that must be considered. These mechanisms will likely necessitate a reduction in the reheating temperature to satisfy the DM constraints. Gravitinos can be produced during reheating from the decay of the inflaton. Moreover, if the gravitino (\tilde{G}) is the LSP the next-to-lightest supersymmetric particle (NLSP) can be the neutralino (χ). Thus, the neutralino is unstable and will undergo gravitational decay via, for instance, $\chi \rightarrow \tilde{G}\gamma$ with a width [19]

$$\Gamma_\chi \sim \frac{m_\chi^3}{M_{\text{P}}^2}. \quad (1.1)$$

¹See also [54–97] for various works on gravitino production and DM.

²Recently, an alternative scenario has gained attention, even within the framework of SUGRA [112–118]: the production of primordial black holes. These black holes could potentially serve as dark matter, despite their non-particle origin.

These late decays, with a timescale of seconds or longer, inject electromagnetic energy, and possible hadrons, through three body channels, like $\chi \rightarrow \tilde{G}W^-\chi^+$, during the BBN epoch and can therefore affect its predictions for the abundances of light elements [48, 119]. Additionally, these decays produce gravitino DM, with

$$\Omega_{3/2}h^2 = \frac{m_{3/2}}{m_\chi} \Omega_\chi h^2. \quad (1.2)$$

For these reasons, in the most realistic models, the value $\Omega_{3/2}h^2 = 0.12$ serves as the upper bound for the thermal DM production, influencing the reheating temperature as we will discuss below.

For the sake of completeness in this discussion, it is worth noting that a similar situation arises in the neutralino DM scenario, where the gravitino can act as the NSLP. In this case, the gravitino is unstable and will decay like [120], $\tilde{G} \rightarrow \chi\gamma$ with a width [18]

$$\Gamma_{\tilde{G}} \sim \frac{m_{3/2}^3}{M_{\text{P}}^2}. \quad (1.3)$$

Similar to the case of gravitino DM, these late decays result in electromagnetic and/or hadronic injections during BBN, affecting its predictions [46, 74] and producing neutralino DM through the equation (1.2), only now as

$$\Omega_\chi h^2 = \frac{m_\chi}{m_{3/2}} \Omega_{3/2} h^2. \quad (1.4)$$

In our discussion of the numerical results below, we will see that if gravitinos constitute all of the DM in the Universe, meaning $\Omega_{3/2}h^2 = \Omega_{\text{DM}}h^2 \sim 0.12$, this imposes strict limits on the reheating temperature. For example, with a gluino mass near the current LHC limit, a reheating temperature of $T_{\text{reh}} \simeq 10^9$ GeV is consistent with a gravitino mass of $m_{3/2} \simeq 1$ TeV.

For higher $M_{1/2}$ values favored by current accelerator and cosmological data, such as $M_{1/2} = 10$ TeV with $m_{3/2} \simeq 1$ TeV, the compatible reheating temperature drops to $T_{\text{reh}} \simeq 10^7$ GeV. If we consider other DM candidates like the neutralino, the constraints on the gravitino can be relaxed, allowing for a much lower reheating temperature. Specifically, for $m_{3/2} \simeq 1$ TeV and $M_{1/2} = 10$ TeV (or $M_{1/2} = 20$ TeV), the upper bound on T_{reh} is reduced to 10^4 GeV (or 10^3 GeV), respectively.

The paper is structured as follows: In section 2, we discuss the general framework of our computation. Section 3 focuses on calculating the $2 \rightarrow 2$ amplitudes and the various components of the production rate. Section 4 presents the overall results, while in section 5, we explore the cosmological implications of our findings, particularly concerning the reheating temperature, which is a crucial factor in calculating other important cosmological quantities, such as the baryon asymmetry. In section 6, we present our conclusions, while the extensive appendices provide all the technical details and methodologies used to obtain our results.

2 General framework

Interactions involving gravitinos, \tilde{G} , are gravitationally suppressed by the inverse of the reduced Planck mass $M_{\text{P}} = (8\pi G)^{-1/2}$ (refer to Appendix A for more details on the gravitino interactions). Consequently, the leading order contributions to gravitino production occur through processes of the form

$$ab \rightarrow c\tilde{G}, \quad (2.1)$$

where a , b , and c can be either three SUSY particles or a combination of one SUSY and two SM particles. Out of ten possible processes, only five need to be explicitly calculated. The remaining five processes can be derived by using crossing symmetries, as we will discuss later. Nevertheless, instead of computing the full amplitudes (\mathcal{M}) for the ten possible processes (see table 1 for the corresponding squared amplitudes for the $\text{SU}(3)_c$ gauge group), i.e.³

$$|\mathcal{M}_{X,\text{full}}|^2 = |\mathcal{M}_{X,s} + \mathcal{M}_{X,t} + \mathcal{M}_{X,u} + \mathcal{M}_{X,x}|^2, \quad (2.2)$$

with $X = A, B, \dots, J$, we will compute the gravitino thermal production rate ($\gamma_{3/2}$) using the following recipe [17]:

$$\gamma_{3/2} = \gamma_{\text{D}} + \gamma_{\text{sub}} + \gamma_{\text{top}}. \quad (2.3)$$

We will briefly discuss the three contributions and provide more details in the following sections.

1. *The D-graph* (γ_{D}): This contribution, illustrated in figure 1 for the case of the gluon-gluino loop, contains the sum of the squared amplitudes for the s , t , and u channels,

$$|\mathcal{M}_{X,D}|^2 = |\mathcal{M}_{X,s}|^2 + |\mathcal{M}_{X,t}|^2 + |\mathcal{M}_{X,u}|^2. \quad (2.4)$$

2. *The subtracted rate* (γ_{sub}): The subtracted rate is the difference between the full amplitudes (2.2) and the amplitudes already contained in the D-graph (2.4), i.e.

$$|\mathcal{M}_{X,\text{sub}}|^2 = |\mathcal{M}_{X,\text{full}}|^2 - |\mathcal{M}_{X,D}|^2. \quad (2.5)$$

3. *The top Yukawa rate* (γ_{top}): This contribution differs from the previously discussed $2 \rightarrow 2$ processes, as it focuses on gravitino production through scatterings involving top quarks.

The reason for performing this decomposition instead of computing directly the full squared amplitudes (2.2) is that if a massless gauge boson is exchanged in the t - or u -channel, the corresponding squared matrix element exhibit infrared (IR) divergences. This occurs in processes B, F, G and H of table 1. The approach described above regularizes these IR divergences. This method was first used in [17] for gravitinos, and in [121] and [122] for axions (see also [123] for an alternative approach) and axinos, respectively. We employed the same procedure in our previous study [20], though the squared amplitudes for some processes differ by certain factors. However, the subtracted components that impact our numerical results remain the same.

³The indices s , t , u denote the diagrams resulting from the exchange of a particle in the respective channel, while the index x stands for the diagram involving a quartic vertex.

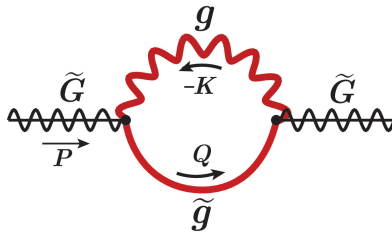


Figure 1. The one-loop thermally corrected gravitino propagator (D-graph). The thick red lines in the graph indicate the gaugino and gauge boson thermally corrected propagators, as discussed in the text.

3 The $2 \rightarrow 2$ processes and their subtracted part

In this section we will discuss the analytical results for the $2 \rightarrow 2$ processes involved in the gravitino production. Following the discussion in the previous section we also present the corresponding results for the subtracted part.

The full amplitude squared is given as

$$|\mathcal{M}_{\text{full}}|^2 = \sum_{X=A}^J |\mathcal{M}_{X,\text{full}}|^2. \quad (3.1)$$

The same holds for $|\mathcal{M}_{\text{sub}}|^2$ and $|\mathcal{M}_{\text{D}}|^2$.

As can be seen in table 1 for the case of the $SU(3)_c$ gauge group the incoming particles a, b and the outgoing c could be gluons g , gluinos \tilde{g} , quarks q or/and squarks \tilde{q} . Similar processes occur in the context of the gauge groups $SU(2)_L$ and $U(1)_Y$. The factor Y_N used in table 1 is defined as

$$Y_N = 1 + \frac{M_N^2}{3m_{3/2}^2}. \quad (3.2)$$

Here and thereafter, the index $N = 1, 2, 3$ will be the gauge group index running over the gauge groups of the SM: $U(1)_Y$, $SU(2)_L$, and $SU(3)_c$. M_N and $m_{3/2}$ represent the gaugino and the gravitino mass, respectively. In Y_N the unity originates from the $3/2$ gravitino components and the mass term from the $1/2$ goldstino part. The Casimir operators appear in this table⁴ are $C_N = \sum_{a,b,c} |f^{abc}|^2 = N(N^2 - 1) = \{0, 6, 24\}$ and $C'_N = \sum_{a,i,j}^\phi |T_{ij}^a|^2 = \{11, 21, 48\}$. With $\sum_{a,i,j}^\phi$ we denote the sum over all involved chiral multiplets and group indices. The f^{abc} are group structure constants and T^a the generators. Please note that the processes A, B and F of table 1 does not appear in $U(1)_Y$, since $C_1 = 0$. Moreover we assume that the particles a, b and c are massless.

The calculation of each of these amplitudes in table 1 consists of two parts: the pure gravitino spin $3/2$ part and the gaugino $1/2$ part. Following [17] for the gravitino

⁴In the thermal bath we have to sum over all incoming and outgoing states, e.g. $\sum_{a,b,c} |f^{abc}|^2 = 3 \times 8 = 24 \equiv C_3$.

X	process	$ \mathcal{M}_{X,\text{full}} ^2$	$ \mathcal{M}_{X,\text{sub}} ^2$
A	$gg \rightarrow \tilde{g}\tilde{G}$	$2C_N(s + 2t + 2t^2/s)$	$-2sC_N$
B	$g\tilde{g} \rightarrow g\tilde{G}$	$-4C_N(t + 2s + 2s^2/t)$	$2tC_N$
C	$\tilde{q}g \rightarrow q\tilde{G}$	$4sC'_N$	0
D	$gq \rightarrow \tilde{q}\tilde{G}$	$-4tC'_N$	0
E	$\tilde{q}q \rightarrow g\tilde{G}$	$-4tC'_N$	0
F	$\tilde{g}\tilde{g} \rightarrow \tilde{g}\tilde{G}$	$4C_N(s^2 + t^2 + u^2)^2/(stu)$	0
G	$q\tilde{g} \rightarrow q\tilde{G}$	$-8C'_N(s + s^2/t)$	0
H	$\tilde{q}\tilde{g} \rightarrow \tilde{q}\tilde{G}$	$-4C'_N(t + 2s + 2s^2/t)$	0
I	$q\bar{q} \rightarrow \tilde{g}\tilde{G}$	$-4C'_N(t + t^2/s)$	0
J	$\tilde{q}\bar{\tilde{q}} \rightarrow \tilde{g}\tilde{G}$	$2C'_N(s + 2t + 2t^2/s)$	0

Table 1. Squared matrix elements for gravitino production in terms of $g_N^2 Y_N/M_{\text{P}}^2$ assuming massless particles, $Y_N = 1 + M_N^2/(3m_{3/2}^2)$, $C_N = \{0, 6, 24\}$ and $C'_N = \{11, 21, 48\}$ and $N = 1, 2, 3$ runs over the SM gauge groups. $|\mathcal{M}_{X,\text{sub}}|^2$ is given in the non-derivative approach, as discussed in the text.

we use the gravitino polarization sum

$$\Pi_{\mu\nu}^{3/2}(P) = \sum_{i=\pm 3/2} \tilde{G}_\mu^{(i)} \bar{\tilde{G}}_\nu^{(i)} = -\frac{1}{2}\gamma_\mu \not{P} \gamma_\nu - \not{P} g_{\mu\nu}, \quad (3.3)$$

where \tilde{G}_μ is the gravitino spinor and P its momentum. For the or the goldstino 1/2 component, we use the non-derivative approach described in [8, 42]. We have proved that the result for the full squared amplitude is the same, either in the derivative or the non-derivative approach [124–126].

It is worth noting that the amplitudes for processes B, F, G and H develop infrared divergences. As discussed earlier, to remove these divergences, we separate the total scattering rate into two parts: the subtracted and the D -graph part. Additionally, for processes with incoming or/and outgoing gauge bosons, we have explicitly checked the gauge invariance of the full amplitudes squared, $|\mathcal{M}_{X,\text{full}}|^2$. On the other hand, $|\mathcal{M}_{X,\text{sub}}|^2$ is gauge dependent. As pointed out in [17], splitting the amplitudes into resummed and non-resummed contributions violates gauge invariance. Therefore, a gauge dependence of the result is expected.

3.1 The squared amplitudes

Many of the interaction terms concerning the gravitino in the full SUGRA Lagrangian [127] are irrelevant for our analysis, since the considered centre of mass energy \sqrt{s} is much lower than the Planck scale M_{P} , thus some operators are suppressed at least by

a factor $\sim 1/M_{\text{P}}$. The relevant interaction Lagrangian⁵ is

$$\begin{aligned}
\mathcal{L}_{3/2, \text{int}}^{(N)} &= -\frac{i}{\sqrt{2}M_{\text{P}}}\bar{G}_\mu S_{\text{MSSM}}^\mu + \text{h.c.} \\
&= -\frac{i}{\sqrt{2}M_{\text{P}}}\left[\mathcal{D}_\mu^{(N)}\phi^{*i}\bar{G}_\nu\gamma^\mu\gamma^\nu\chi_L^i - \mathcal{D}_\mu^{(N)}\phi^i\bar{\chi}_L^i\gamma^\nu\gamma^\mu\tilde{G}_\nu\right] \\
&\quad -\frac{i}{8M_{\text{P}}}\bar{G}_\mu[\gamma^\rho, \gamma^\sigma]\gamma^\mu\lambda^{(N)a}F_{\rho\sigma}^{(N)a},
\end{aligned} \tag{3.4}$$

where in the first line S_{MSSM}^μ denotes the contribution from MSSM to the supercurrent. In the following, we will use this to calculate the relevant squared amplitudes.

It is worth noting that by applying crossing symmetry, one can observe that out of the ten squared amplitudes, only five are independent; namely, A, C, F, G, and H. The remaining amplitudes, B, D, E, I, and J, can be derived from these using crossing symmetry. The explicit analytic forms of the amplitudes A, C, F, G, and H, along with their corresponding Feynman diagrams, are presented in Appendix A. Additionally, the involved vertices are described, and instructions are provided for deriving the squared amplitudes for the other processes, B, D, E, I, and J, using crossing symmetry.

We consider the (massless) vector particles in the R_ξ gauge with $\xi = 1$. To ensure accuracy, we have verified the results involving external vector particles by also employing the axial gauge. The subtracted part is gauge-dependent and is presented in the $\xi = 1$ gauge. Additionally, the spin-1/2 component of the gravitino is calculated using both the derivative and non-derivative approaches, with full results found to be consistent across methods. The subtracted part is provided exclusively in the non-derivative approach.

3.2 The subtracted rate

In the fourth column of table 1, we present the subtracted part for each process, expressed in terms of $g_N^2 Y_N/M_{\text{P}}^2$ and assuming massless particles. This contribution includes the sum of the interference terms among the four types of diagrams (s , t , u , x) and the squared x -diagram. It is non-zero only for the processes A and B. In [17], the subtracted part for processes H and J is also non-zero. We assume the authors used the squark-squark-gluino-goldstino Feynman rule from [7], which lacks a γ_5 factor. In contrast, we use the correct Feynman rule from [8], leading to a zero result for processes H and J.

To calculate the subtracted part of thermal rate $ab \rightarrow c\tilde{G}$, we use the expression:

$$\gamma_{\text{sub}} \equiv \mathcal{C} = \frac{1}{(2\pi)^8} \int \frac{d^3\mathbf{p}_a}{2E_a} \frac{d^3\mathbf{p}_b}{2E_b} \frac{d^3\mathbf{p}_c}{2E_c} \frac{d^3\mathbf{p}}{2E} |\mathcal{M}|^2 f_a f_b (1 \pm f_c) \delta^4(P_a + P_b - P_c - P), \tag{3.5}$$

where f_i are the usual Bose-Einstein or Fermi-Dirac distributions given by:

$$f_{B/F} = \frac{1}{e^{\frac{E}{T}} \mp 1}. \tag{3.6}$$

⁵In this context, ϕ , \tilde{G} , χ , λ , and F represent the bosons, gravitino, fermions, gauginos, and field strength, respectively.

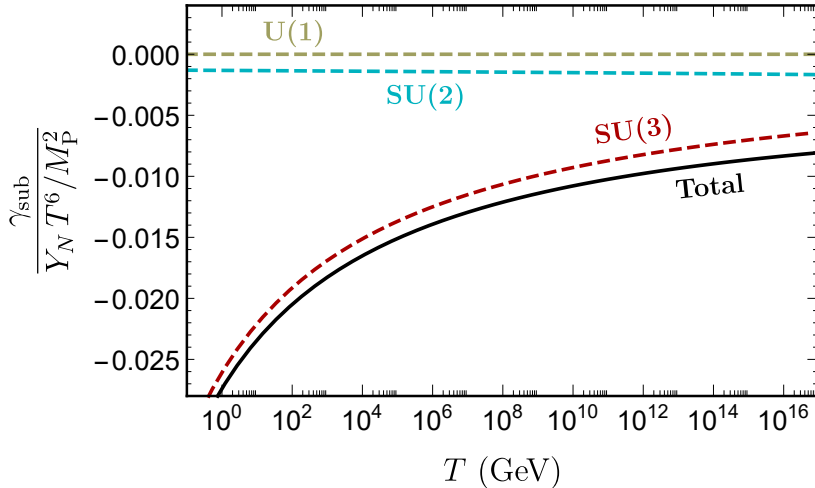


Figure 2. The subtracted rate given by (3.9) normalized by $Y_N T^6 / M_P^2$. The curves represent, in order, the total subtracted rate and the contributions from $SU(3)_c$, $SU(2)_L$, and $U(1)_Y$.

In the relevant temperature range, all particles except the gravitino are in thermal equilibrium. As implied in the equation above, the statistical factor $f_{\tilde{G}}$ for the gravitino is negligible, allowing us to approximate $1 - f_{\tilde{G}} \sim 1$. Additionally, backward reactions can be neglected, as they are proportional to $f_{\tilde{G}}$.

A remark with respect to our notation is in order: we use the symbol γ for the thermal production rate and \mathcal{C} for the same quantity, as calculated for the $2 \rightarrow 2$ processes in Appendix C. Both represent the same quantity, which serves as the source term in the Boltzmann equation (5.1).

Please note that by approximating $1 \pm f_c \sim 1$, we can solve equation (3.5) analytically. However, in our calculation, we retain the $1 \pm f_c$ factor in the integral, necessitating a numerical computation of the collision term \mathcal{C} . The detailed numerical method is provided in Appendix C. If we use the amplitudes computed in the non-derivative approach (refer to Appendix A.4.2), we see that the only nonzero contributions are those of processes A and B, which are

$$|\mathcal{M}_{A,\text{sub}}|^2 = \frac{1}{2} \frac{g_N^2}{M_P^2} \left(1 + \frac{M_N^2}{3m_{3/2}^2} \right) (-2sC_N), \quad (3.7)$$

$$|\mathcal{M}_{B,\text{sub}}|^2 = \frac{g_N^2}{M_P^2} \left(1 + \frac{M_N^2}{3m_{3/2}^2} \right) (2tC_N). \quad (3.8)$$

Note that in (3.7) a factor of 1/2 is already included due to the 2 identical incoming particles. Substituting (3.7) and (3.8) in (3.5), the subtracted rate reads as

$$\gamma_{\text{sub}} = \frac{T^6}{M_P^2} \sum_{N=1}^3 g_N^2 \left(1 + \frac{M_N^2}{3m_{3/2}^2} \right) C_N (-\mathcal{C}_{\text{BBF}}^s + 2\mathcal{C}_{\text{BFB}}^t). \quad (3.9)$$

The numerical factors⁶, calculated using the Cuba library [128], are $\mathcal{C}_{\text{BFB}}^s = 0.260 \times 10^{-3}$ and $\mathcal{C}_{\text{BFB}}^t = -0.133 \times 10^{-3}$. The subscripts B and F indicate whether the particles are bosons or fermions, respectively, while the superscripts denote whether the squared amplitude is proportional to s or t . Our result for the subtracted part is negative, which is not unphysical because it is the total rate, not the subtracted part, that must be positive. In figure 2, we show the total subtracted rate (black solid line) along with the contributions from individual gauge groups (colored dashed lines) as a function of temperature, spanning from 1 to 10^{16} GeV.

We observe that the subtracted contribution γ_{sub} includes thermal corrections proportional to T^6 . Later, in the gravitino self-energy contribution (D -graph), we will implement thermal corrections to the gaugino and fermion propagators, which include higher orders of T by performing a Dyson summation.

In the previous calculations, it was assumed that $m_{3/2}$ is much smaller than T . In the limit where $m_{3/2} \rightarrow 0$, the gravitino interaction Lagrangian with the supercurrent S_μ^{MSSM} becomes

$$\mathcal{L}_{3/2,\text{int}} = \frac{-i}{\sqrt{2}M_{\text{P}}} \tilde{G}^\mu S_\mu^{\text{MSSM}} \xrightarrow{m_{3/2} \rightarrow 0} \frac{-i}{\sqrt{2}M_{\text{P}}} \tilde{G}_{(3/2)}^\mu S_\mu^{\text{MSSM}} - \frac{i}{\sqrt{3}M_{\text{P}}} \frac{\bar{\chi}(\partial^\mu S_\mu^{\text{MSSM}})}{m_{3/2}}, \quad (3.10)$$

where it is assumed that in this limit, the gravitino decomposes as [17, 129–132]

$$\tilde{G}^\mu \xrightarrow{m_{3/2} \rightarrow 0} \tilde{G}_{(3/2)}^\mu - \frac{i}{\sqrt{6}} \gamma^\mu \chi - \sqrt{\frac{2}{3}} \frac{\partial^\mu \chi}{m_{3/2}}, \quad (3.11)$$

and the goldstino coupling has been neglected. The \tilde{G}^μ represents the full gravitino spinor and $\tilde{G}_{(3/2)}^\mu$ the pure spin-3/2 gravitino components, while χ is the spin-1/2 goldstino component, both of which are massless in this limit. The sum of the pure gravitino components of $\tilde{G}_{(3/2)}^\mu$ is given in equation (3.3). This decomposition in equation (3.11) is the basis both for the derivative, and the non-derivative approaches presented in Appendices A.4.1 and A.4.2, respectively.

It should be noted that in [17], they approximate that the amplitude squared and the rate γ decompose similarly, as

$$\gamma(\tilde{G}^\mu) \simeq \gamma(\tilde{G}_{(3/2)}^\mu) + \gamma(\chi). \quad (3.12)$$

The equality is not exact due to the omission of “interference” terms, which are considered small.

3.3 Top Yukawa contribution to the thermal rate

For the calculation of γ_{top} we need the part of the amplitudes for⁷ $t\bar{t} \rightarrow \tilde{H}_2^0 \tilde{G}$ and $\tilde{t}_i \tilde{t}_j^* \rightarrow \tilde{H}_2^0 \tilde{G}$ which is proportional to the top Yukawa coupling y_t in the limit of massless

⁶Here we present only the numerical factors $\mathcal{C}_{\text{BFB}}^s$ and $\mathcal{C}_{\text{BFB}}^t$ required for this calculation. In Appendix C we also provide the coefficients for amplitudes proportional to s^2 , t^2 , and st for various combinations of the involved particles. For more details, see table 5.

⁷The particle \tilde{H}_2^0 denotes the superpartner of the Higgs field H_2^0 , the Higgsino.

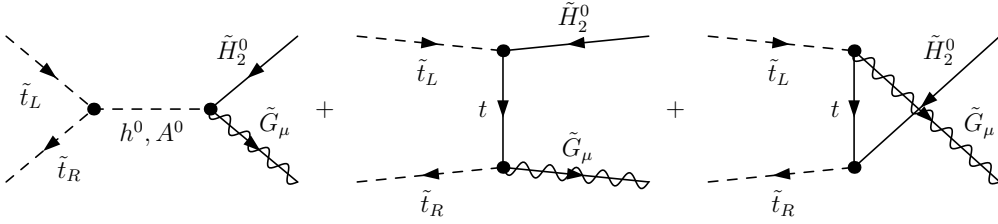


Figure 3. Feynman graphs for the process $\tilde{t}_L \tilde{t}_R^* \rightarrow \tilde{H}_2^0 \tilde{G}$.

particles compared to the energy of the thermal bath. The contribution from $t\bar{t} \rightarrow \tilde{H}_2^0 \tilde{G}$ vanishes and $\tilde{t}_i \tilde{t}_j^*$ becomes $\tilde{t}_L \tilde{t}_R^*$ or $\tilde{t}_R \tilde{t}_L^*$. The Feynman graphs for the contributing amplitudes for $\tilde{t}_L \tilde{t}_R^*$ are shown in figure 3. Note that the graph with the four-point coupling of $\tilde{t}_R \tilde{t}_L^* \tilde{H}_2^0 \tilde{G}$ is zero in the $\xi = -2$ gauge for \tilde{G} . The amplitudes for $\tilde{t}_L \tilde{t}_R^* \rightarrow \tilde{H}_2^0 \tilde{G}$ are

$$A^H = -\frac{\sqrt{2} c_F y_t A_t}{M_{\text{P}} s} p_1^\mu \bar{u}_\mu(p_2) P_L v(p_1), \quad (3.13)$$

$$A^{\text{top}} = -\frac{\sqrt{2} c_F y_t}{M_{\text{P}}} \left(\frac{k_1^\mu}{u} - \frac{k_2^\mu}{t} \right) \bar{u}_\mu(p_2) \not{k}_1 P_L v(p_1), \quad (3.14)$$

where A^H corresponds to the left Feynman graph in figure 3, which is the sum of the graphs with h^0 and A^0 s-channel exchange, and A^{top} to the sum of the two other graphs in figure 3. The graph with H^0 s-channel exchange vanishes in that limit. The colour factor c_F is δ_{rs} with r the colour of \tilde{t}_L and s the colour of \tilde{t}_L^* . Note, $|c_F|^2 = 3$, and A_t is the trilinear soft breaking term in the stop sector.

We start from the amplitudes (3.13) and (3.14), and calculate the squared amplitudes for $\tilde{t}_L \tilde{t}_R^* \rightarrow \tilde{H}_2^0 \tilde{G}$. For the spin $\pm 3/2$ contribution we use the gravitino polarization sum (3.3). Only the two graphs with top propagator contribute,

$$|A^{\text{top}}|^2 \rightarrow |A^{\frac{3}{2}}|^2 = \frac{3y_t^2}{M_{\text{P}}^2} s. \quad (3.15)$$

For the spin $\pm 1/2$ contribution we work in the derivative approach, and apply the rule (A.50) to (3.13) and (3.14). Only the graphs with h^0 and A^0 propagators contribute,

$$|A^H|^2 \rightarrow |A^{\frac{1}{2}}|^2 = \frac{y_t^2}{M_{\text{P}}^2} \frac{A_t^2}{m_{3/2}^2} s. \quad (3.16)$$

For $\tilde{t}_R \tilde{t}_L^* \rightarrow \tilde{H}_2^0 \tilde{G}$ we get the same results. Thus, the squared amplitude in order y_t^2 for the calculation of γ_{top} is

$$|A|^2 = |A^{\frac{3}{2}}|^2 + |A^{\frac{1}{2}}|^2 = \frac{6y_t^2}{M_{\text{P}}^2} \left(1 + \frac{A_t^2}{3m_{3/2}^2} \right) s. \quad (3.17)$$

This result is smaller by a factor of 12 compared to the one given in [17]. The top Yukawa rate, which is the collision term (3.5), with $|\mathcal{M}|^2 \equiv |A|^2$, is

$$\gamma_{top} = \frac{T^6}{M_{\text{P}}^2} 6 C_{BBF}^s y_t^2 \left(1 + \frac{A_t^2}{3m_{3/2}^2} \right), \quad (3.18)$$

with $C_{BBF}^s = 0.260 \times 10^{-3}$, see table 5.

3.4 Thermally corrected gravitino self-energy

As outlined in Section 2, equation (2.5) describes the relation between the thermally corrected gravitino self-energy, the so-called D -graph, and the sum of squared amplitudes for the channels s , t , and u . In our analysis⁸ of the D -graph, we incorporate resummed thermal corrections to the gauge boson and gaugino propagators⁹. Although figure 1 specifically depicts the gluino-gluon thermal loop, our study encompasses contributions from all gauge groups. The momentum flow used in calculating the D -graph is illustrated in figure 1. That is $\tilde{G}(P) \rightarrow g(K) + \tilde{g}(Q)$, with

$$P = (p, p, 0, 0), \quad K = (k_0, k \cos \theta_k, k \sin \theta_k, 0), \quad \text{and} \quad Q = (q_0, q \cos \theta_q, q \sin \theta_q, 0), \quad (3.19)$$

where $\theta_{k,q}$ are the polar angles of the corresponding 3-momenta \mathbf{k} and \mathbf{q} in spherical coordinates. Here, we have already assumed that the gravitino is massless compared to the high temperature of the thermal bath, that is $P^2 = 0$.

We have seven variables: p, k, q, k_0, q_0, c_k , and c_q , and three non-trivial equations due to the overall momentum conservation, $P^i = K^i + Q^i$, $i = 0, 1, 2$. Thus, we are left with 4 independent variables. Using the momentum conservation we obtain that

$$p = k_0 + q_0, \quad (3.20)$$

$$\cos \theta_k = \frac{p^2 - q^2 + k^2}{2kp}, \quad (3.21)$$

$$\cos \theta_q = \frac{p^2 + q^2 - k^2}{2pq}, \quad (3.22)$$

$$\cos(\theta_k - \theta_q) = \frac{p^2 - q^2 - k^2}{2kq}. \quad (3.23)$$

In order to calculate the gravitino selfenergy with vector-gaugino loop in the massless case we need the Feynman rules for the two vertices. Thus, the goldstino selfenergy with gluon-gluino loop including the outer goldstino legs can be written as

$$\Pi = \frac{n_3}{8M_{\text{P}}^2} \frac{M_3^2}{3m_{3/2}^2} \int \frac{d^4 K}{(2\pi)^4} \text{Tr} (\not{P}[\not{K}, \gamma^\mu] S(Q) [\not{K}, \gamma^\nu] D_{\mu\nu}(K)), \quad (3.24)$$

⁸In this section, we closely follow the notation of [17].

⁹Similar to [17], where the gravitino polarization sum (3.3) was utilized to nullify the corresponding quark-squark D -graph.

Gauge group	N_V	N_F	N_S
$U(1)_Y$	0	11	22
$SU(2)_L$	2	9	14
$SU(3)_c$	3	9	12

Table 2. The numerical factors involved in the expressions for the vector-boson propagators. Each value corresponds to a particular gauge group, $U(1)_Y$, $SU(2)_L$ or $SU(3)_c$, assuming the MSSM particle content.

in which $S(Q)$ is the gluino propagator, $D_{\mu\nu}(K)$ the gluon propagator, and $n_3 = 8$ from the color running in the loop. Now, we can easily generalize that to the expression $\Pi^<$, including all three groups, $U(1)_Y$, $SU(2)_L$ and $SU(3)_c$, with $n_1 = 1$ and $n_2 = 3$. As we use the non-time ordered selfenergy $\Pi^<$, we get an additional factor of $1/2$, that is

$$\Pi^<(P) = \frac{1}{16M_P^2} \sum_{N=1}^3 n_N \left(1 + \frac{M_N^2}{3m_{3/2}^2} \right) \int \frac{d^4K}{(2\pi)^4} \text{Tr} \left(\not{P}[\not{K}, \gamma^\mu] {}^*S^<(Q)[\not{K}, \gamma^\nu] {}^*D_{\mu\nu}^<(K) \right), \quad (3.25)$$

with the thermally resummed propagators denoted by a $*$,

$${}^*S^<(Q) = \frac{f_F(q_0)}{2} [(\gamma_0 - \gamma^i \hat{q}^i) \rho_+(Q) + (\gamma_0 + \gamma^i \hat{q}^i) \rho_-(Q)], \quad (3.26)$$

$${}^*D_{\mu\nu}^<(K) = f_B(k_0) \left[\Pi_{\mu\nu}^T \rho_T(K) + \Pi_{\mu\nu}^L \frac{k^2}{K^2} \rho_L(K) + \xi \frac{K_\mu K_\nu}{K^4} \right], \quad (3.27)$$

with $\hat{q}^i = q^i/q$. In (3.25) we have also incorporated the helicity $\pm 3/2$ components of the gravitino, as in [6] it has been shown, up to two loop order in the gauge couplings, that one obtains the characteristic factor $1 + M_N^2/3m_{3/2}^2$, as well as in the calculation of the $2 \rightarrow 2$ scatterings. The spectral functions (longitudinal and transverse) for gauge-bosons are given by [133, 134]

$$\rho_L = -2 \frac{P^2}{p^2} \text{Im} \left(\frac{1}{P^2 - \pi_0 - \pi_L} \right), \quad \rho_T = -2 \text{Im} \left(\frac{1}{P^2 - \pi_0 - \pi_T} \right), \quad (3.28)$$

where the longitudinal-transverse thermal, and the $T = 0$ corrections to the vector propagator are given by

$$\pi_L = - \frac{P^2}{p^2} g_N^2 (N_S H_S + N_F H_F + N_V H_V) \stackrel{\text{HTL}}{\sim} - \frac{P^2}{p^2} (L+1) m_V^2, \quad (3.29a)$$

$$\pi_T = - \frac{\pi_L}{2} + \frac{g_N^2}{2} (N_S g_3 + N_F G_F + N_V G_V) \stackrel{\text{HTL}}{\sim} \left(1 + \frac{P^2}{p^2} \frac{L+1}{2} \right) m_V^2, \quad (3.29b)$$

$$\pi_0 = g_N^2 P^2 \frac{2N_F + N_S/2 - 5N_V}{48\pi^2} \ln \left(- \frac{P^2}{\mu^2} \right). \quad (3.29c)$$

In equations above, the HTL refers to the hard thermal loop approximation, which is valid at energies and momenta $p, p_0 \ll T$. It accurately describes the thermal effects

that occur at $p, p_0 \sim g_N T$ when $g_N \ll 1$. However, this approximation does not hold for physical gauge couplings, particularly for the strong coupling g_3 . Note also that π_L and π_T do not contain the one-loop quantum correction at $T = 0$, so it must be added separately.

The integrals $H_{S,F,V}, G_{S,F,V}$ and the function L can be found in Appendix B, while the numerical factors $N_{S,F,V}$ are given in table 2 assuming the MSSM particle content. The vector thermal mass is given by

$$m_V^2 = \frac{1}{6} g_N^2 T^2 (N_V + N_S/2 + N_F/2). \quad (3.30)$$

For fermion particles (ρ_+) and fermion holes (ρ_-) the spectral functions, including the $T = 0$ contribution, are given by

$$\rho_{\pm} = -\text{Im} \left\{ \left(\omega_{\mp} \left[1 + \frac{1}{2\pi^2} \frac{m_F^2}{T^2} \left(2 - \ln \left(-\frac{P^2}{\mu^2} \right) \right) \right] + \frac{m_F^2}{T^2} F_{\pm} \right)^{-1} \right\}, \quad \omega_{\pm} = \frac{p_0 \pm p}{2}, \quad (3.31)$$

where the thermal fermion mass is

$$m_F^2 = \left(\frac{g_N^2 C_R}{8} + \frac{\lambda_q^2}{16} \right) T^2, \quad (3.32)$$

and

$$F_{\pm} = \mp \int_0^{\infty} \frac{dk}{\pi^2} \left[\frac{\omega_{\mp}}{p^2} \left(k L_+(n_B + n_F) + L_-(n_B \omega_{\mp} + n_F \omega_{\pm}) \right) + 2 \frac{L \omega_{\mp} + \omega_{\pm}}{pp_0} k (n_B + n_F) \right] \stackrel{\text{HTL}}{\sim} \mp \frac{T^2}{2} \frac{L \omega_{\mp} + \omega_{\pm}}{pp_0}. \quad (3.33)$$

The statistical factors $n_{B,F}$ are given by (3.6) by substituting $E \rightarrow |E|$, while the group factor $C_R = \{1, 3/4, 4/3\}$ [135] and λ_q is the scalar-fermion-fermion coupling (see equation (B.8)).

Both the vector and fermion spectral functions¹⁰ can be decomposed as

$$\rho_{L,T} = \rho_{L,T}^{\text{pole}} + \rho_{L,T}^{\text{cont}}, \quad \rho_{\pm} = \rho_{\pm}^{\text{pole}} + \rho_{\pm}^{\text{cont}}, \quad (3.34)$$

where the continuum contribution is computed directly from the definitions in equations (3.28) and (3.31). To compute the pole contribution, one must solve the dispersion relations to determine the pole positions and calculate the residues at these poles. In [17], the HTL approximation was assumed to obtain analytical results for the pole positions and residues. In our work, however, we utilize numerical methods to solve the full one-loop dispersion relations (as detailed in Appendix B.3), without relying on the HTL approximation. This approach allows us to compute both the pole positions and residues using the complete one-loop thermal corrections.

¹⁰Note that the temperature dependence of the spectral functions is $\rho_{L,T} \sim T^{-2}$ and $\rho_{\pm} \sim T^{-1}$.

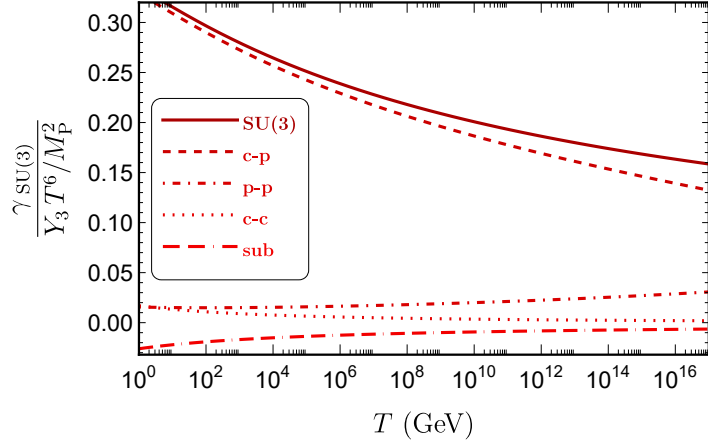


Figure 4. Various contributions to the $SU(3)_c$ production rate, normalized by $Y_N T^6 / M_{\text{P}}^2$, are shown. The solid line represents the total result, while the other lines correspond to the “cont-pole”, “pole-pole”, “cont-cont” and subtracted contributions, respectively.

Using the parametrization (3.19) and the abbreviations “c” and “s” for cosine and sine, we get for the different spectral function combinations of equation (3.25) the following results:

$$\propto \rho_- \rho_L : 16 p k^2 (c_{2k} c_q + s_{2k} s_q + 1), \quad (3.35)$$

$$\propto \rho_+ \rho_L : 16 p k^2 (-c_{2k} c_q - s_{2k} s_q + 1), \quad (3.36)$$

$$\propto \rho_- \rho_T : 16 p ((k_0^2 + k^2)(2 - \cos(2\theta_k - \theta_q) - c_q) - 4k_0 k (c_k - \cos(\theta_k - \theta_q))), \quad (3.37)$$

$$\propto \rho_+ \rho_T : 16 p ((k_0^2 + k^2)(2 + \cos(2\theta_k - \theta_q) + c_q) - 4k_0 k (c_k + \cos(\theta_k - \theta_q))). \quad (3.38)$$

After some algebra equation (3.25) becomes

$$\begin{aligned} \Pi^<(P) = & \frac{1}{32M_{\text{P}}^2} \sum_{N=1}^3 n_N \left(1 + \frac{M_N^2}{3m_{3/2}^2} \right) \int \frac{d^4 K}{(2\pi)^4} f_F(q_0) f_B(k_0) \times \\ & \left[\rho_L(K) \rho_-(Q) 32 p k^2 \cos^2 \frac{2\theta_k - \theta_q}{2} + \rho_L(K) \rho_+(Q) 32 p k^2 \sin^2 \frac{2\theta_k - \theta_q}{2} \right. \\ & + \rho_T(K) \rho_-(Q) 16 p ((k_0^2 + k^2)(2 - \cos(2\theta_k - \theta_q) - c_q) - 4k_0 k (c_k - \cos(\theta_k - \theta_q))) \\ & \left. + \rho_T(K) \rho_+(Q) 16 p ((k_0^2 + k^2)(2 + \cos(2\theta_k - \theta_q) + c_q) - 4k_0 k (c_k + \cos(\theta_k - \theta_q))) \right]. \end{aligned} \quad (3.39)$$

In order to compute the integral (3.39) it is convenient to multiply by the 4-momentum δ -function $\int d^4 Q \delta^4(K + Q - P) = 1$. Also, using the relations

$$d^4 K = dk_0 k^2 dk d \cos \theta_k d\phi_k \quad \text{and} \quad d^4 Q = dq_0 q^2 dq d \cos \theta_q d\phi_q, \quad (3.40)$$

we can perform the integrations dq_0 , $d \cos \theta_q$, $d \cos \theta_k$ and $d\phi_k$ thanks to the δ -function. Nothing depends on $d\phi_k$, so we get an extra 2π from this integration. After these

integrations the equations (3.35)-(3.38) become,

$$\propto \rho_- \rho_L : \frac{8}{q} (p-q)^2 ((p+q)^2 - k^2), \quad (3.41)$$

$$\propto \rho_+ \rho_L : \frac{8}{q} (p+q)^2 (k^2 - (p-q)^2), \quad (3.42)$$

$$\propto \rho_- \rho_T : \frac{8}{q} (k^2 - (p-q)^2) \left(\left(1 + \frac{k_0^2}{k^2}\right) (k^2 + (p+q)^2) - 4k_0(p+q) \right), \quad (3.43)$$

$$\propto \rho_+ \rho_T : \frac{8}{q} ((p+q)^2 - k^2) \left(\left(1 + \frac{k_0^2}{k^2}\right) (k^2 + (p-q)^2) - 4k_0(p-q) \right), \quad (3.44)$$

and the resummed propagator (3.39) takes the form

$$\begin{aligned} \Pi^<(P) &= \frac{1}{4(2\pi)^3} \frac{1}{M_{\text{P}}^2} \sum_{N=1}^3 n_N \left(1 + \frac{M_N^2}{3m_{3/2}^2} \right) \int_{-\infty}^{\infty} dk_0 \int_0^{\infty} dk \int_{|k-p|}^{k+p} dq \frac{k}{p} f_B(k_0) f_F(p_0 - k_0) \\ &\times \left[\rho_L(K) \rho_-(Q) (p-q)^2 ((p+q)^2 - k^2) + \rho_L(K) \rho_+(Q) (p+q)^2 (k^2 - (p-q)^2) \right. \\ &+ \rho_T(K) \rho_-(Q) (k^2 - (p-q)^2) \left(\left(1 + \frac{k_0^2}{k^2}\right) (k^2 + (p+q)^2) - 4k_0(p+q) \right) \\ &\left. + \rho_T(K) \rho_+(Q) ((p+q)^2 - k^2) \left(\left(1 + \frac{k_0^2}{k^2}\right) (k^2 + (p-q)^2) - 4k_0(p-q) \right) \right], \quad (3.45) \end{aligned}$$

with $q_0 = p - k_0$. In order to compute the production rate γ_D we will use its definition [133, 134]

$$\gamma_D = \int \frac{d^3\mathbf{p}}{2p_0(2\pi)^3} \Pi^<(p), \quad (3.46)$$

with $d^3\mathbf{p} = 4\pi p^2 dp$ in this frame. Then

$$\begin{aligned} \gamma_D &= \frac{1}{4(2\pi)^5} \frac{1}{M_{\text{P}}^2} \sum_{N=1}^3 n_N \left(1 + \frac{M_N^2}{3m_{3/2}^2} \right) \times \\ &\int_0^{\infty} dp \int_{-\infty}^{\infty} dk_0 \int_0^{\infty} dk \int_{|k-p|}^{k+p} dq k f_B(k_0) f_F(p_0 - k_0) \times \\ &\left[\rho_L(K) \rho_-(Q) (p-q)^2 ((p+q)^2 - k^2) + \rho_L(K) \rho_+(Q) (p+q)^2 (k^2 - (p-q)^2) \right. \\ &+ \rho_T(K) \rho_-(Q) (k^2 - (p-q)^2) \left(\left(1 + \frac{k_0^2}{k^2}\right) (k^2 + (p+q)^2) - 4k_0(p+q) \right) \\ &\left. + \rho_T(K) \rho_+(Q) ((p+q)^2 - k^2) \left(\left(1 + \frac{k_0^2}{k^2}\right) (k^2 + (p-q)^2) - 4k_0(p-q) \right) \right]. \quad (3.47) \end{aligned}$$

The spectral functions $\rho_{L,T}$ and ρ_{\pm} are provided in equations (3.28) and (3.31). The thermally corrected one-loop self-energies for gauge bosons, scalars, and fermions, utilized in the calculation of these spectral functions, are detailed in Appendices B.1

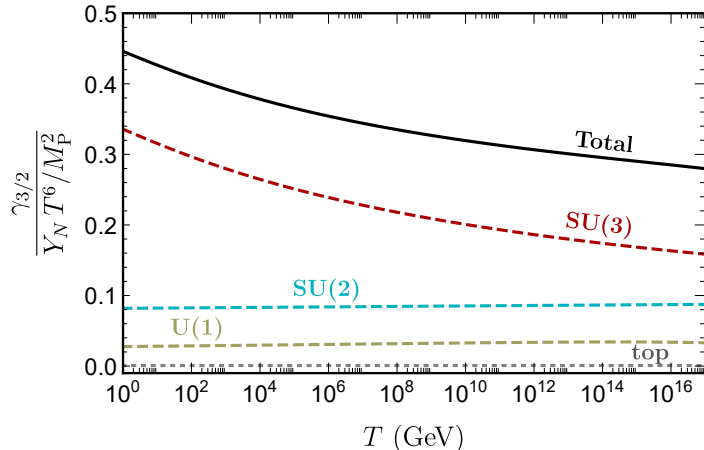


Figure 5. The gravitino production rate normalized by $Y_N T^6 / M_P^2$. The curves represent, in order, the total rate given by (2.3), the $SU(3)_c$, $SU(2)_L$, and $U(1)_Y$ contributions given by (4.1), and the top Yukawa rate given by (3.18). The top Yukawa coupling is $y_t = 0.7$.

and B.2, and are also available in various previous works [135–140]. Comparing our result with that of [17], we observe differences in the overall factor and the number of independent phase-space integrations. Our analytical result has been verified using various frames for the momentum flow into the loop. The four dimensional integral (3.47) has been calculated numerically using the Cuba library [128]. In this computation, the products of the different spectral densities yield contributions of the forms “pole-pole”, “cont-pole”, and “cont-cont”. Consequently, we must evaluate integrals of dimensions two, three, and four, respectively, due to the presence of δ -functions associated with the pole parts of the spectral densities. Figure 4 illustrates the various contributions to the production rate for the $SU(3)_c$ group. Among these, the “cont-pole” contribution is the most significant, surpassing the other contributions. In figure 5 we show the full gravitino production rate (black solid line) given by equation (2.3) in terms of the factor $Y_N T^6 / M_P^2$. The dashed lines represent the individual contributions from each gauge group, while the gray dotted line shows the top quark contribution¹¹ given by equation (3.18). Compared to previous works that implement the same method for computing the gravitino production rate [17, 20], our updated results show a decrease of approximately 25–30% across the entire temperature range when compared to [17]. Relative to [20], we observe a reduction of about 40% at $T \sim 1$ GeV. This reduction decreases with rising temperatures, reaching around 20% at $T \sim 10^8$ GeV, and disappears entirely at the grand unification (GUT) scale 2×10^{16} GeV.

In the following section, we will introduce a useful parametrization of this integral, inspired by [36]. This parametrization incorporates the subtracted rate calculated in section 3.2, providing a more refined approach to the integral’s evaluation.

¹¹Note that the top quark contribution in figure 5 is normalized by $(1 + A_t^2 / 3m_{3/2}^2) T^6 / M_P^2$.

Gauge group	c_N	k_N	Gauge group	ξ_N	σ_N	τ_N
$U(1)_Y$	35.56	0.85	$U(1)_Y$	0.93	60.38	2.30
$SU(2)_L$	35.33	1.38	$SU(2)_L$	10.14	188.33	3.72
$SU(3)_c$	29.40	3.07	$SU(3)_c$	2.81	12.73	1.02

Table 3. The values of the constants c_N, k_N (left) and ξ_N, σ_N, τ_N (right) that parametrize our result for the subtracted and the D-graph part. Each value corresponds to a particular gauge group, $U(1)_Y$, $SU(2)_L$, and $SU(3)_c$.

4 The total gravitino thermal production rate

Since the computation of the gravitino production rate presented in figure 5 is purely numerical, it would be useful to have some practical parametrizations. Ellis et al. [36] were the first to parametrize the results of [17] using the gauge coupling constants g_N , and we applied a similar approach in [20]. Therefore, we have parametrized the results for the subtracted part and the D-graph using the gauge couplings g_Y, g_2 , and g_3 . Specifically,

$$\gamma_{\text{sub}} + \gamma_{\text{D}} = \frac{3\zeta(3)T^6}{16\pi^3 M_{\text{P}}^2} \sum_{N=1}^3 c_N g_N^2 \left(1 + \frac{M_N^2}{3m_{3/2}^2} \right) \ln \left(\frac{k_N}{g_N} \right), \quad (4.1)$$

where the constants c_N depend on the gauge group and their values are given in table 3 (left). By adding the contribution proportional to h_t , we obtain the total gravitino thermal production rate

$$\gamma_{3/2} = \frac{T^6}{M_{\text{P}}^2} \left[\frac{3\zeta(3)}{16\pi^3} \sum_{N=1}^3 c_N g_N^2 \left(1 + \frac{M_N^2}{3m_{3/2}^2} \right) \ln \left(\frac{k_N}{g_N} \right) + 6 \mathcal{C}_{BBF}^s y_t^2 \left(1 + \frac{A_t^2}{3m_{3/2}^2} \right) \right], \quad (4.2)$$

where from table 5 we get $\mathcal{C}_{BBF}^s = 0.260 \times 10^{-3}$. The detailed calculation of this factor can be found in Appendix C. It is worth noting that $\gamma_{3/2}$ is related to the thermalized cross section $\langle \sigma v_{\text{rel}} \rangle$, as

$$\gamma_{3/2} = \langle \sigma v_{\text{rel}} \rangle n_{\text{rad}}^2, \quad (4.3)$$

where $n_{\text{rad}} = \zeta(3)T^3/\pi^2$.

The above parametrization can be rewritten in a more convenient form as a function of temperature rather than coupling constants, as follows:

$$\gamma_{\text{sub}} + \gamma_{\text{D}} = \sum_{N=1}^3 \frac{T^6}{M_{\text{P}}^2} \left(\xi_N \frac{\ln(\sigma_N \pm \ln T) - \tau_N}{\sigma_N \pm \ln T} \right) \left(1 + \frac{M_N^2}{3m_{3/2}^2} \right), \quad (4.4)$$

where the plus sign corresponds to $SU(3)_c$ and the minus sign to $SU(2)_L$ and $U(1)_Y$ respectively. The temperature T is measured in GeV and the constants ξ_N, σ_N and τ_N are given in table 3 (right). The above equation for the total width $\gamma_{3/2}$ reads as

$$\gamma_{3/2} = \frac{T^6}{M_{\text{P}}^2} \left[\sum_{N=1}^3 \left(\xi_N \frac{\ln(\sigma_N \pm \ln T) - \tau_N}{\sigma_N \pm \ln T} \right) \left(1 + \frac{M_N^2}{3m_{3/2}^2} \right) + 6 \mathcal{C}_{BBF}^s y_t^2 \left(1 + \frac{A_t^2}{3m_{3/2}^2} \right) \right]. \quad (4.5)$$

In (4.4) we did not introduce a new parametrization. Instead, we substituted the leading-order logarithmic corrections to the running of all the gauge couplings [141], assuming a unified gauge coupling $g_{\text{GUT}} = \sqrt{\pi/6}$ at the GUT scale. Note also that the gaugino masses are temperature-dependent and are assumed to unify at the same GUT scale, with the values $M_N = M_{1/2} (g_N^2/g_{\text{GUT}}^2)$.

5 Gravitino abundance, DM and reheating temperature

The gravitinos are produced after inflation mainly by three mechanisms: through decays of the inflaton field [31–38], directly non-thermally through decays of heavier unstable supersymmetric particles, like gauginos or sfermions [49–53] and last but not least thermally through $1 \rightarrow 2$ or $2 \rightarrow 2$ processes with a gravitino in the final state [5–12, 16, 17, 20, 36, 40–44]. Apparently, for the later the most important ingredient is the gravitino thermal production rate calculated in equation (4.1).

In order to obtain the thermal gravitino abundance one has to solve the Boltzmann equation for the gravitino number density $n_{3/2}$

$$\frac{dn_{3/2}}{dt} + 3Hn_{3/2} = \gamma_{3/2}, \quad (5.1)$$

where H is the Hubble constant. The gravitino abundance $Y_{3/2}$ is defined as

$$Y_{3/2} = \frac{n_{3/2}}{n_{\text{rad}}}, \quad (5.2)$$

where we have used for the radiation density $n_{\text{rad}} = \zeta(3)T^3/\pi^2$. Substituting $Y_{3/2}$ into (5.1) we get the Boltzmann equation for $Y_{3/2}$

$$\frac{dY_{3/2}}{dt} + 3 \left(H + \frac{1}{T} \frac{dT}{dt} \right) Y_{3/2} = \frac{\gamma_{3/2}}{n_{\text{rad}}}. \quad (5.3)$$

Using the entropy conservation relation

$$\frac{d(g_{*s}T^3a^3)}{dt} = 0, \quad (5.4)$$

where g_{*s} are the effective entropy degrees of freedom and a the scale factor, we can trade time with temperature in equation (5.3) as

$$\frac{dY_{3/2}}{dT} - Y_{3/2} \frac{d \ln g_{*s}}{dT} = - \frac{\gamma_{3/2}}{HT n_{\text{rad}}} \left[1 + \frac{T}{3} \frac{d \ln g_{*s}}{dT} \right]. \quad (5.5)$$

By integrating equation (5.5) from T_{reh} down to temperature T and assuming that inflaton decay and thermalization are instantaneous and simultaneous at T_{reh} , one gets

$$Y_{3/2}(T) = Y_{3/2}(T_{\text{reh}}) \frac{g_{*s}(T)}{g_{*s}(T_{\text{reh}})} - g_{*s}(T) \int_{T_{\text{reh}}}^T d\tau \frac{\gamma_{3/2}(\tau)}{g_{*s}(\tau) H(\tau) n_{\text{rad}}(\tau) \tau} \left[1 + \frac{\tau}{3} \frac{d \ln g_{*s}(\tau)}{d\tau} \right]. \quad (5.6)$$

Furthermore, applying the standard freeze-in scenario assuming negligible initial gravitino abundance at T_{reh} , $Y_{3/2}(T_{\text{reh}}) \simeq 0$, and ignoring a weak temperature dependence of the integrand in the r.h.s. of (5.6), we get that the gravitino abundance in the limit $T \ll T_{\text{reh}}$ reads as [36]

$$Y_{3/2}(T) \xrightarrow{T \ll T_{\text{reh}}} \frac{\gamma_{3/2}(T_{\text{reh}})}{H(T_{\text{reh}})} \frac{g_{*s}(T)}{g_{*s}(T_{\text{reh}})}. \quad (5.7)$$

We notice that in [36, 84], it has been estimated that the approximation of the instantaneous inflaton decays and the thermalization can affect the result of the gravitino DM abundance by $\sim 10\%$.

Moreover, using the definitions

$$\Omega_{3/2} = \frac{\rho_{3/2}}{\rho_{\text{cr}}}, \quad \rho_{3/2} = n_{3/2} m_{3/2}, \quad (5.8)$$

and the equations (5.2), (5.7) and (4.2), one gets $\Omega_{3/2} h^2$ as

$$\begin{aligned} \Omega_{3/2} h^2 &= \frac{\rho_{3/2}(t_0) h^2}{\rho_{\text{cr}}} = \frac{m_{3/2} Y_{3/2}(T_0) n_{\text{rad}}(T_0) h^2}{\rho_{\text{cr}}} \simeq 1.33 \times 10^{24} \frac{m_{3/2} \gamma_{3/2}(T_{\text{reh}})}{T_{\text{reh}}^5} \\ &\simeq 0.016 \left(\frac{m_{3/2}}{1 \text{ TeV}} \right) \left(\frac{T_{\text{reh}}}{10^{10} \text{ GeV}} \right) \left[\sum_{N=1}^3 c_N g_N^2 \left(1 + \frac{M_N^2}{3m_{3/2}^2} \right) \ln \left(\frac{k_N}{g_N} \right) \right. \\ &\quad \left. + 0.214 y_t^2 \left(1 + \frac{A_t^2}{3m_{3/2}^2} \right) \right]. \end{aligned} \quad (5.9)$$

Here, $\rho_{\text{cr}} = 3 H_0^2 M_{\text{P}}^2$ is the critical energy density, $H_0 = 100 h \text{ km}/(\text{s Mpc})$ is the Hubble constant, and $T_0 = 2.7K$ is the current temperature of the cosmic microwave background. The entropy degrees of freedom at the relevant temperatures are $g_{*s}(T_0) = 43/11$ and $g_{*s}(T_{\text{reh}}) = 915/4$. The latter value corresponds to the effective energy degrees of freedom for $H(T_{\text{reh}})$ in the MSSM.

Following the latest data from the Planck satellite, the cosmological accepted value for the DM density in the Universe is $\Omega_{\text{DM}} h^2 = 0.12 \pm 0.0012$ [142]. Assuming that the thermal gravitino abundance accounts for the total observed DM in the Universe, we can derive bounds on the gravitino mass and/or the reheating temperature. However, as we will see, these bounds significantly weaken when allowing for other particles to play the role of the DM particle.

Before presenting our numerical results, it is helpful to first discuss the various DM candidates in SUGRA and how their mass hierarchy can ultimately impact the reheating temperature. In extensively studied models like mSUGRA and CMSSM, the neutralino is the primary DM candidate, aside from the gravitino. For example, in the CMSSM framework, where supersymmetry breaking is gravity mediated, gauge couplings and soft masses are unified at the GUT scale, and radiative electroweak symmetry breaking occurs, the neutralino mass m_χ is typically up to $\sim 1/2$ of the common gaugino mass $M_{1/2}$. The neutralino is a mixture of bino (\tilde{B}), neutral wino

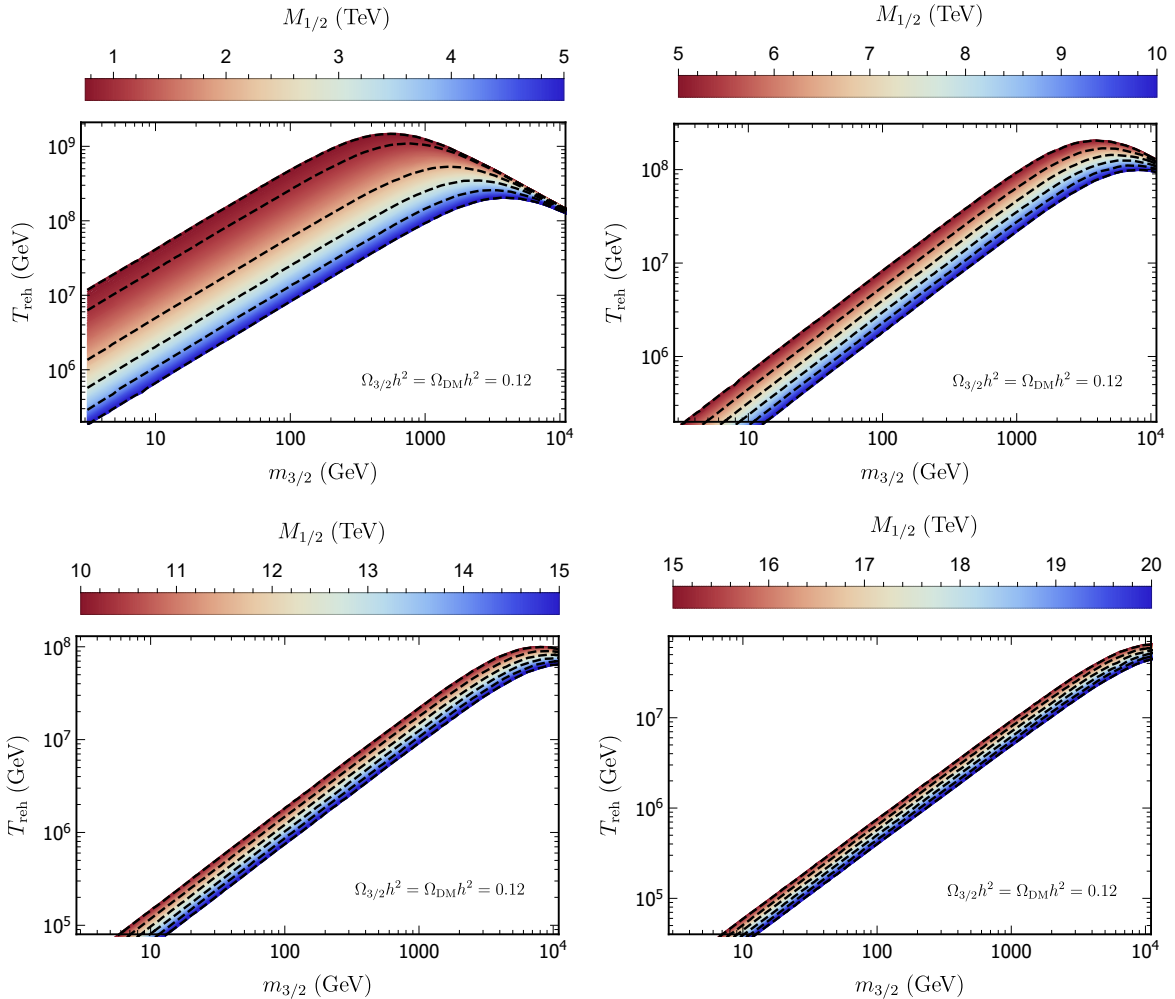


Figure 6. The reheating temperature as a function of gravitino mass for fixed gravitino thermal abundance $\Omega_{3/2}h^2 = \Omega_{\text{DM}}h^2 = 0.12$. The dashed curves, correspond to the values of $M_{1/2}$: (a) from 750 GeV to 5 TeV (upper left panel), (b) from 5 TeV to 10 TeV (upper right panel), (c) from 10 TeV to 15 TeV (lower left panel), and (d) from 15 TeV to 20 TeV (lower right panel), as described in the text. The trilinear coupling A_t is neglected, and the top Yukawa coupling is $y_t = 0.7$.

(\tilde{W}^3), and the neutral Higgsinos (\tilde{H}_1^0) and (\tilde{H}_2^0). In particular, if the neutralino is predominantly bino, then $m_\chi \simeq 0.45 M_{1/2}$. However, if it is mostly Higgsino, its mass is closer to $m_\chi \simeq 0.3 M_{1/2}$.

In figure 6 we plot the reheating temperature as a function of the gravitino mass, having fixed the gravitino abundance to $\Omega_{3/2}h^2 = 0.12$, for four ranges of $M_{1/2}$: (a) from 750 GeV to 5 TeV, (b) from 5 TeV to 10 TeV, (c) from 10 TeV to 15 TeV and (d) from 15 TeV to 20 TeV. In the calculation of the gauge couplings and gaugino masses involved in equation (5.9), we assume gauge coupling unification and a universal gaugino mass $M_{1/2}$ at the GUT scale $\sim 2 \times 10^{16}$ GeV. Moreover, in equation (3.18) the trilinear coupling A_t is neglected and the top Yukawa coupling is $y_t = 0.7$. The

dashed curves in the upper left plot, figure 6 (a), correspond to the values, $M_{1/2} = 750$ GeV, 1, 2, 3, 4 and 5 TeV, respectively. In the subsequent plots, we have included a contour for every 1 TeV.

Based on figure 6 (a), a few comments on the dependence of T_{reh} as a function of $m_{3/2}$ for various values of $M_{1/2}$ and fixed $\Omega_{3/2}h^2$, are in order. First, for large gravitino masses $m_{3/2} \simeq 10^4$ GeV all these curves converge to “the point” $T_{\text{reh}} \simeq 10^8$ GeV. This is because, for such large $m_{3/2}$ and fixed $\Omega_{3/2}h^2$, the reheating temperature is almost independent of $M_{1/2}$, as the factor $M_N^2/(3m_{3/2}^2)$ in equation (5.9) becomes negligible. Second, we observe that for $M_{1/2} \leq 3$ TeV and $m_{3/2} \leq 1$ TeV, the term $M_N^2/(3m_{3/2}^2)$ in equation (5.9) leads to an increasing T_{reh} as a function of $m_{3/2}$. However, for $m_{3/2} > 1$ TeV this term is subdominant, causing T_{reh} to eventually decrease. For this reason the curves appear to have a maximum for the values of $M_{1/2}$ we are plotting. Eventually, for higher values of $M_{1/2}$ the $M_N^2/(3m_{3/2}^2)$ dominates over unity in equation (5.9), causing the maximum to disappear and leaving only a behavior where T_{reh} is almost proportional to $m_{3/2}$. This can be seen in figure 6 (b), (c) and (d).

Moreover, assuming that $M_{1/2} = 750$ GeV, as indicated by recent LHC data [143, 144] on gluino searches, we can deduce from figure 6 (a) that for a maximum $T_{\text{reh}} \simeq 10^9$ GeV, the corresponding gravitino mass is $m_{3/2} \simeq 550$ GeV. On the other hand, taking $M_{1/2} = 5$ TeV the maximum reheating temperature is reduced by almost an order of magnitude to $T_{\text{reh}} \simeq 2 \times 10^8$ GeV. However, this temperature corresponds to much heavier gravitino $m_{3/2} \simeq 3$ TeV.

As shown in figure 6 (a) to (d), higher values of $M_{1/2}$ for the same gravitino mass result in lower reheating temperatures (T_{reh}). For instance, with $m_{3/2} = 1$ TeV, we find that T_{reh} is greater than 10^8 GeV for $M_{1/2}$ up to 5 TeV, whereas T_{reh} falls within the range of 5×10^6 GeV $< T_{\text{reh}} < 8 \times 10^6$ GeV for 15 TeV $< M_{1/2} < 20$ TeV. In addition, we would like to emphasize that although our analysis does not assume a specific supersymmetry-breaking scenario, such as gravity mediation in the CMSSM, adopting such a framework would impact the results. Specifically, there are regions in each plot in figure 6 where the lightest neutralino is lighter than the gravitino. For instance, in panel (a), with $M_{1/2} = 1$ TeV and assuming $m_\chi \simeq 500$ GeV, the corresponding dashed curve above this value does not correspond to a gravitino dark matter scenario in the CMSSM. These “neutralino” dark matter regions shrink as $M_{1/2}$ increases in the subsequent panels. Nevertheless, since we have not committed ourselves to this particular SUSY model, our discussion remains general, even though these regions are considered valid.

In figure 7 we display the thermal gravitino density $\Omega_{3/2}h^2$ as a function of the reheating temperature T_{reh} for five values of the gravitino mass: 1, 10, 100 GeV and 1, 10 TeV, corresponding to the slanted lines in each plot. We present six plots for $M_{1/2} = 750$ GeV, 2, 4, 10, 15, 20 TeV, arranged from the top left window to the bottom right, respectively. Such high values of $M_{1/2}$ are favoured in regions of the parameter space of CMSSM [3] or its extensions [145], where all the current essential direct and indirect constraints are satisfied. Assuming that the entire DM of the Universe is due to thermally produced gravitinos, we have marked the 3σ cosmologically allowed region by the gray horizontal thick line. However, we also show values of $\Omega_{3/2}h^2$ much

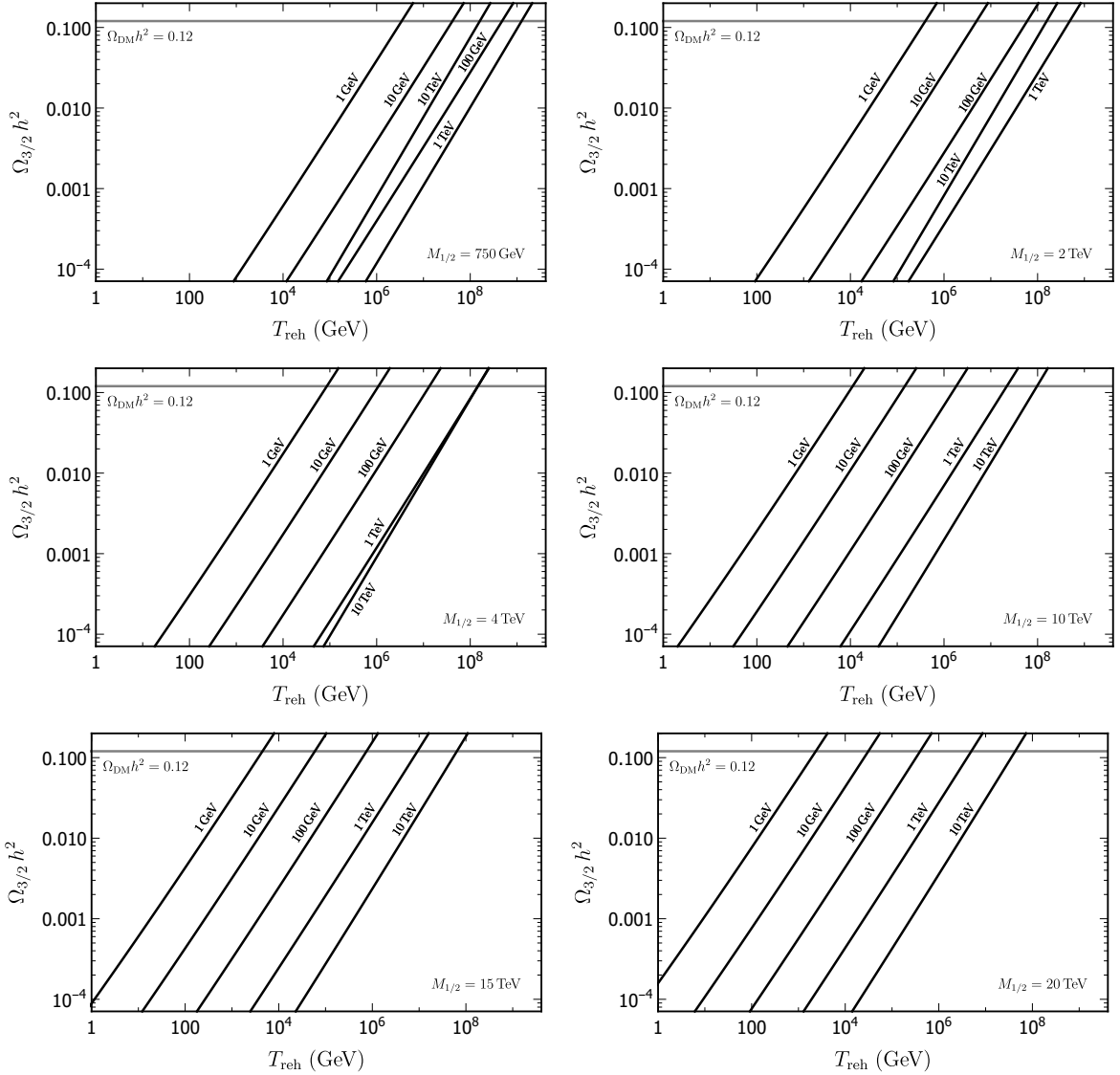


Figure 7. The thermal gravitino density, $\Omega_{3/2} h^2$, is shown as a function of the reheating temperature, T_{reh} , for various gravitino masses ranging from 1 GeV to 10 TeV. The universal gaugino mass, $M_{1/2}$, varies from 750 GeV (top left) to 20 TeV (bottom right). The gray horizontal thick line represents the cosmologically allowed DM density, $\Omega_{3/2} h^2 = \Omega_{\text{DM}} h^2 = 0.12 \pm 0.0012$.

lower from this value, under the assumption that the gravitino is not the main DM particle. For instance, as discussed in the Introduction, this scenario can be realised in SUGRA-based models, where the neutralino is the LSP of the model.

The discussion we have had for figure 6 will help us understand the relative positions of the lines in the plots in figure 7. Let's start with the first plot for $M_{1/2} = 750$ GeV. Assuming $\Omega_{3/2} = \Omega_{\text{DM}}$, we get $T_{\text{reh}} \simeq 10^9$ GeV for $m_{3/2} = 1$ TeV, as expected from figure 6 (a). Relaxing the DM constraint in this case, we notice that the reheating temperature can be reduced by at least three order of magnitudes to

$T_{\text{reh}} \lesssim 10^6$ GeV. The same applies to all $m_{3/2}, M_{1/2}$ values (slanted lines) in these plots.

However in the first plot, it is interesting to note that the line for $m_{3/2} = 10$ TeV is to the left of the lines for $m_{3/2} = 100$ GeV and $m_{3/2} = 1$ TeV. This again results from the maximum observed in figure 6 (a), as discussed above, which leads to a smaller T_{reh} for $m_{3/2} = 10$ TeV compared to $m_{3/2} = 100$ GeV. The same pattern is observed in the plot for $M_{1/2} = 2$ TeV. In the plot for $M_{1/2} = 4$ TeV, the lines for $m_{3/2} = 1$ TeV and $m_{3/2} = 10$ TeV almost coincide. The last three plots of figure 7, where $m_{3/2} > 5$ TeV, the expected order of the lines appears. These correspond to figure 6 (b), (c) and (d), where the maximum has almost disappeared.

As anticipated, if the entire DM content is not attributed solely to the thermal abundance of gravitinos, the upper bounds on the reheating temperature are significantly lowered. This reduction can be achieved through various methods. One approach involves considering alternative DM candidates, such as axions or axinos. Specifically, within the frameworks of minimal SUGRA model or CMSSM, if the gravitino is the LSP, it can also be generated through the late decays of NLSP, like gauginos (neutralino) or sfermions. Consequently, the thermal abundance of gravitinos may only contribute a portion of the total DM density in the Universe. Similar to figure 6, figure 7 also features lines that, within the context of the CMSSM, correspond to a neutralino DM scenario. For instance, in the first plot, assuming $m_\chi \simeq 500$ GeV the lines corresponding to $m_{3/2} = 1$ TeV, 10 TeV fall within this category. As discussed in the introduction, since our model is SUGRA-based, gravitinos continue to be produced thermally but eventually decay with a width given by equation (1.3), contributing to the total neutralino DM through equation (1.4). Consequently, in this scenario, the T_{reh} inferred from figure 7 is significantly lower than what would be required if $\Omega_{\text{DM}} h^2 = 0.12$.

6 Conclusions

In this paper, we have calculated the gravitino production rate and its thermal abundance, using the complete one-loop thermally corrected gravitino self-energy. We have refined the main analytical formulas for the gravitino decay rate and computed it numerically without approximation, appropriately parameterizing the final results. Within the framework of minimal supergravity models, assuming gaugino mass unification, we have updated the bounds on the reheating temperature for specific gravitino masses.

Assuming that gravitinos constitute the entirety of the dark matter in the Universe, $\Omega_{3/2} h^2 = \Omega_{\text{DM}} h^2 \sim 0.12$, imposes stringent constraints on the reheating temperature. For instance, with a gluino mass at the current LHC limit, we find that a maximum reheating temperature of $T_{\text{reh}} \simeq 10^9$ GeV is compatible with a gravitino mass of $m_{3/2} \simeq 1$ TeV. Moreover, with a reheating temperature an order of magnitude lower, $T_{\text{reh}} \simeq 10^8$ GeV, the common gaugino mass $M_{1/2}$ can range up to 2-4 TeV within the same gravitino mass range.

For much higher values of $M_{1/2}$ which are favored by current accelerator and cosmological data in the context of supersymmetric models, e.g., $M_{1/2} = 10$ TeV, and $m_{3/2} \simeq 1$ TeV, the reheating temperature that is compatible with the gravitino DM scenario, is $T_{\text{reh}} \simeq 10^7$. Allowing for the possibility that other particles, such as the neutralino, can play the role of dark matter, we can relax the gravitino DM constraint. In this case the reheating temperature can be much smaller. Specifically, for $m_{3/2} \simeq 1$ TeV and $M_{1/2} = 10$ TeV ($M_{1/2} = 20$ TeV) we obtain an upper bound for the reheating temperature $T_{\text{reh}} \lesssim 10^4$ TeV ($T_{\text{reh}} \lesssim 10^3$ TeV), respectively.

It should be noted that applying constraints on gravitino dark matter scenarios using T_{reh} implies the assumption of thermal leptogenesis as the mechanism for generating baryon asymmetry. However, many alternative models for baryogenesis exist. Additionally, as previously highlighted, the thermal gravitino abundance is only a part of the total abundance, which impacts the phenomenological analysis. Moreover, our results for the gravitino decay rate and its abundance can be applied within a general supersymmetric framework, regardless of the specifics of the supersymmetry-breaking scenario

Acknowledgments

The work of IDG was supported by the Estonian Research Council grants MOB3JD1202, RVTT3, RVTT7, and by the CoE program TK202 “Fundamental Universe”. The work of V.C.S. was partially supported by the Hellenic Foundation for Research and Innovation (H.F.R.I.) under the “First Call for H.F.R.I. Research Projects to support Faculty members and Researchers and the procurement of high-cost research equipment grant” (Project Number: 824). V.C.S. is grateful to the William I. Fine Theoretical Physics Institute at the University of Minnesota for their financial support and the warm hospitality extended to him during his sabbatical leave. He also acknowledges support from the Simons Foundation Targeted Grant 920184 to the William I. Fine Theoretical Physics Institute.

A Amplitudes

A.1 Couplings

The involved interactions to the gravitino \tilde{G} can be found e.g. in [19]. The SM and MSSM interactions are given in corresponding textbooks. But for completeness and simplicity we list all involved interactions below.

The $gg\tilde{g}\tilde{G}$ interaction is

$$\mathcal{L} = -\frac{i}{8M_{\text{P}}} (2\partial_\rho G_\sigma^a - g_3 f^{abc} G_\rho^b G_\sigma^c) \left(\tilde{G}_\mu [\gamma^\rho, \gamma^\sigma] \gamma^\mu \tilde{g}^a + \tilde{g}^a \gamma^\mu [\gamma^\rho, \gamma^\sigma] \tilde{G}_\mu \right). \quad (\text{A.1})$$

Note that the vertex rule of $g_\mu^a g_\nu^b \tilde{g}^c \tilde{G}_\rho$ gets an additional factor of 2,

$$\text{Vertex}(g_\mu^a g_\nu^b \tilde{g}^c \tilde{G}_\rho) = -\frac{i g_3}{4M_{\text{P}}} f^{abc} \gamma^\rho [\gamma^\mu, \gamma^\nu]. \quad (\text{A.2})$$

The vertex rule for $g_\mu^a g_\nu^b \tilde{G}_\rho$ can also be deduced from (A.1), with $i\partial_\mu \rightarrow p_\mu$ (incoming). The three-gluon vertex, defined by the Lagrangian $\mathcal{L} = -g_3 f^{abc} G^{b\nu} G^{c\mu} (\partial_\nu G_\mu^a)$ is

$$\text{Vertex}(g_\mu^a g_\nu^b g_\rho^c) = -\frac{g_3}{4M_{\text{P}}} f^{abc} V^{\mu\nu\rho}(k_1, k_2, k_3), \quad (\text{A.3})$$

with all momenta defined incoming, and

$$V^{\mu\nu\rho}(k_1, k_2, k_3) = (k_1 - k_2)^\rho g^{\mu\nu} + (k_2 - k_3)^\mu g^{\nu\rho} + (k_3 - k_1)^\nu g^{\mu\rho}. \quad (\text{A.4})$$

For the $\xi = 1$ gauge we also will need the coupling of the FP-ghosts to the gluon. The Lagrangian is

$$\mathcal{L} = -g_3 f_{abc} (\partial \bar{\eta}^a) G^{c\mu} \eta^b, \quad (\text{A.5})$$

with $\bar{\eta} = \eta^*$. Note that the η and $\bar{\eta}$ are anti-commuting scalar fields. The gluon- η - $\bar{\eta}$ vertex is

$$\text{Vertex}(g_\mu^c \rightarrow \eta^a(k_2) \bar{\eta}^b) = -g_3 f_{abc} k_{2\mu}. \quad (\text{A.6})$$

Next we have the $g\tilde{g}\tilde{g}$ interaction. The Lagrangian is

$$\mathcal{L} = \frac{i}{2} g_3 f_{abc} G_\mu^a \tilde{g}^b \gamma^\mu \tilde{g}^c \quad (\text{A.7})$$

with e. g.

$$\text{Vertex}(g_\mu^a \tilde{g}_\nu^b \tilde{g}^c) = -g_3 f_{abc} \epsilon_\mu(k_0) \bar{u}(k_1) \gamma^\mu v(k_2), \quad (\text{A.8})$$

taking $\tilde{g}(k_1)$ as outgoing particle and $\tilde{g}(k_2)$ as outgoing antiparticle. Note the additional factor 2 due to the Majorana structure of \tilde{g} .

Now we turn to systems involving strong interacting quarks and squarks. We will use the shortcuts

$$\alpha_{RL}^i = R_{iL} P_R - R_{iR} P_L, \quad (\text{A.9})$$

$$\alpha_{LR}^i = R_{iL} P_L - R_{iR} P_R, \quad (\text{A.10})$$

and define the conjugated expressions as

$$\alpha_{RL}^{i*} \equiv R_{iL}^* P_R - R_{iR}^* P_L, \quad (\text{A.11})$$

$$\alpha_{LR}^{i*} \equiv R_{iL}^* P_L - R_{iR}^* P_R, \quad (\text{A.12})$$

in the convention $\tilde{q}_i = R_{i\alpha}$, $i = 1, 2$; $\alpha = L, R$. For massless squarks $\tilde{q}_1 = \tilde{q}_L$ and $\tilde{q}_2 = \tilde{q}_R$, $R_{1L} = R_{2R} = 1$, $R_{1R} = R_{2L} = 0$.

The $q\tilde{q}\tilde{g}$ interaction is given by

$$\mathcal{L} = -\sqrt{2}g_3 T_{st}^a (\bar{q}^s \alpha_{RL}^{i*} \tilde{g}^a \tilde{q}_i^t + \bar{\tilde{g}}^a \alpha_{LR}^i q^t \tilde{q}_i^{*s}), \quad (\text{A.13})$$

and $q\tilde{q}\tilde{G}$ by

$$\mathcal{L} = \frac{1}{\sqrt{2}M_P} \delta_{rt} \left[\bar{q}^r \gamma^\nu \gamma^\mu \alpha_{RL}^{i*} \tilde{G}_\nu (i\partial_\mu \tilde{q}_i^t) - \bar{\tilde{G}} \gamma^\mu \gamma^\nu \alpha_{LR}^i q^t (i\partial_\mu \tilde{q}_i^{*r}) \right]. \quad (\text{A.14})$$

We also need the qqg and $\tilde{q}\tilde{q}g$ interactions,

$$\mathcal{L} = -g_3 T_{st}^a G_\mu^a \bar{q}^s \gamma^\mu q^t, \quad (\text{A.15})$$

$$\mathcal{L} = -g_3 T_{st}^a G_\mu^a \tilde{q}_i^{*s} \left[(\partial^\mu \tilde{q}_j) - (\partial^\mu \tilde{q}_i^{*s}) \tilde{q}_j \right] \delta_{ij}, \quad (\text{A.16})$$

with e.g. the rule for

$$\text{Vertex}(\tilde{q}_i^r(k_1) \rightarrow g^a + \tilde{q}_j^s(k_2)) = -ig_3 T_{rs}^a (k_1 + k_2)_\mu \delta_{ij}. \quad (\text{A.17})$$

A.2 Kinematics

Before we go into the details of the individual channels we fix the kinematics by

$$P_1(k_1) + P_2(k_2) \rightarrow P_3(p_1) + \tilde{G}(p_2), \quad (\text{A.18})$$

with the particles $P_{1,2,3}$ and the overall momenta relation $k_1 + k_2 = p_1 + p_2$. The Mandelstam variables are fixed by

$$s = (k_1 + k_2)^2 = (p_1 + p_2)^2, \quad (\text{A.19})$$

$$t = (k_1 - p_1)^2 = (k_2 - p_2)^2, \quad (\text{A.20})$$

$$u = (k_1 - p_2)^2 = (k_2 - p_1)^2, \quad (\text{A.21})$$

together with $s + t + u = \sum_{i=1}^4 M_i^2$. In general, we can have three types of crossing symmetries in the amplitudes,

$$P_1 \leftrightarrow P_2 : k_1 \leftrightarrow k_2 \quad \dots \quad s \text{ unchanged}, t \leftrightarrow u, \quad (\text{A.22})$$

$$P_1 \leftrightarrow P_3 : k_1 \leftrightarrow p_1 \quad \dots \quad t \text{ unchanged}, s \leftrightarrow -u, \quad (\text{A.23})$$

$$P_2 \leftrightarrow P_3 : k_2 \leftrightarrow p_1 \quad \dots \quad u \text{ unchanged}, s \leftrightarrow -t, \quad (\text{A.24})$$

assuming massless particles. In the cases where crossing symmetries are possible, we will discuss them in the following sections. Furthermore the case (A.22) is of no relevance because interchanging P_1 with P_2 will give the same cross section. Note that for (A.23) and (A.24) we have particle \leftrightarrow antiparticle. The gluon g and the gluino \tilde{g} , which is a Majorana particle, remain unchanged.

A.3 Involved interactions

In what follows we present the $|\mathcal{M}_{X,\text{full}}|^2$ for the above processes as it is also shown in table 1. We begin by focusing exclusively on the $\text{SU}(3)_c$ results (see figures. 8 - 13). All results for $|\mathcal{M}_i|^2 (i = A, \dots, J)$ are presented in terms of $g_3^2 Y_3 / M_{\text{P}}^2$, with Y_3 defined in (3.2).

• Amplitudes for $\tilde{g}\tilde{g} \rightarrow \tilde{g}\tilde{G}$ (process F)

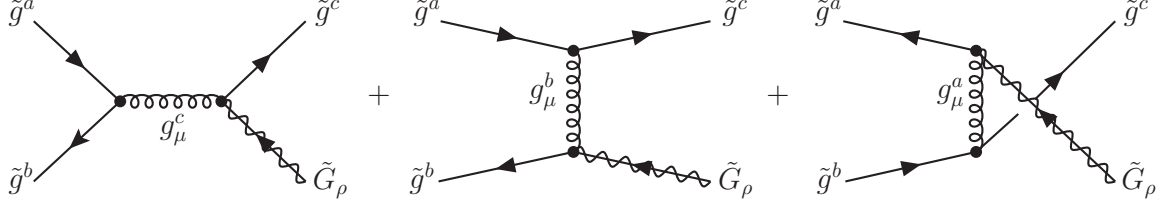


Figure 8. Feynman graphs for the process $\tilde{g}\tilde{g} \rightarrow \tilde{g}\tilde{G}$.

There are three Feynman diagrams, with a g propagator in the s -channel (1), t -channel (2) and u -channel (3). Here one has to be careful because \mathcal{M}_2 gets an additional minus sign from fermion statistics.

$$\mathcal{M}_1 = -\frac{g_3}{4M_{\text{P}s}} f_{abc} \bar{v}(k_2) \gamma_\mu u(k_1) \bar{u}(p_1) \gamma^\rho [k_1 + k_2, \gamma^\mu] v_\rho(p_2), \quad (\text{A.25})$$

$$\mathcal{M}_2 = \frac{g_3}{4M_{\text{P}t}} f_{abc} \bar{u}(p_1) \gamma_\mu u(k_1) \bar{v}(k_2) \gamma^\rho [p_1 - k_1, \gamma^\mu] v_\rho(p_2), \quad (\text{A.26})$$

$$\mathcal{M}_3 = -\frac{g_3}{4M_{\text{P}u}} f_{abc} \bar{u}(p_1) \gamma_\mu u(k_2) \bar{v}(k_1) \gamma^\rho [k_2 - p_1, \gamma^\mu] v_\rho(p_2). \quad (\text{A.27})$$

The full amplitude squared, with fixed a, b, c , is

$$|\mathcal{M}_{F,\text{full}}|^2 = -8 \frac{(s^2 + st + t^2)^2}{st(s+t)} |f^{abc}|^2 \rightarrow 8C_3 \frac{(s^2 + t^2 + u^2)^2}{stu}, \quad (\text{A.28})$$

where we used that $s + t = -u$ and $|f^{abc}|^2 \rightarrow C_3 = 24$ for $\text{SU}(3)_c$. The factor of $1/2$, accounting for the identical incoming gluinos, is already included. Note that there is no crossing channel possible, because we get for the interchanges (A.22) - (A.24) always the same sum of amplitudes.

• Amplitudes for $g\tilde{g} \rightarrow \tilde{g}\tilde{G}$ (process A)

There are four Feynman diagrams, (1): with the four-point interaction, (2): with a g propagator in the s -channel, (3): a \tilde{g} propagator in the t -channel, and (4): a \tilde{g}

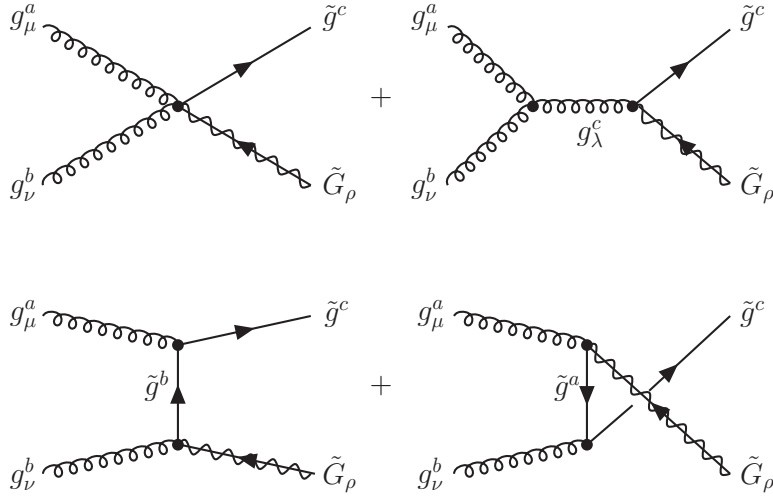


Figure 9. Feynman graphs for the process $gg \rightarrow \tilde{g}\tilde{G}$.

propagator in the u -channel,

$$\mathcal{M}_1 = -\frac{g_3}{4M_{\text{P}}} f_{abc} \bar{u}(p_1) \gamma^\rho [\gamma^\mu, \gamma^\nu] v_\rho(p_2) \epsilon_\mu(k_1) \epsilon_\nu(k_2). \quad (\text{A.29})$$

$$\mathcal{M}_2 = \frac{g_3}{4M_{\text{P}} s} f_{abc} V^{\mu\nu\delta}(k_1, k_2, -k_1 - k_2) \bar{u}(p_1) \gamma^\rho [k_1 + k_2, \gamma_\delta] v_\rho(p_2) \epsilon_\mu(k_1) \epsilon_\nu(k_2), \quad (\text{A.30})$$

$$\mathcal{M}_3 = \frac{g_3}{4M_{\text{P}}} \frac{f_{abc}}{t - m_{\tilde{g}}^2} \bar{u}(p_1) \gamma^\mu (k_2 - \not{p}_2 + m_{\tilde{g}}) \gamma^\rho [k_2, \gamma^\nu] v_\rho(p_2) \epsilon_\mu(k_1) \epsilon_\nu(k_2), \quad (\text{A.31})$$

$$\mathcal{M}_4 = -\frac{g_3}{4M_{\text{P}}} \frac{f_{abc}}{u - m_{\tilde{g}}^2} \bar{u}(p_1) \gamma^\nu (k_1 - \not{p}_2 + m_{\tilde{g}}) \gamma^\rho [k_1, \gamma^\mu] v_\rho(p_2) \epsilon_\mu(k_1) \epsilon_\nu(k_2). \quad (\text{A.32})$$

For the $\xi = 1$ gauge we also need the matrix elements with the incoming FP-ghosts

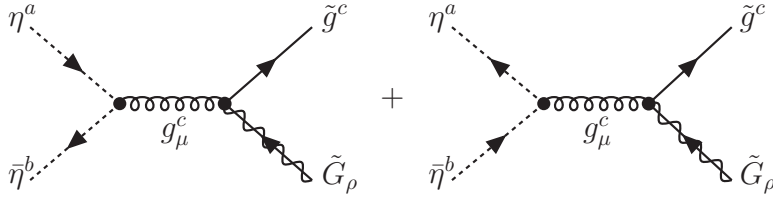


Figure 10. Feynman graph with FP-ghosts in the $\xi = 1$ gauge for the process A.

for the gluon. There are two graphs possible,

$$\mathcal{M}_\eta = \frac{g_3}{4M_{\text{P}}} f_{abc} \bar{u}(p_1) \gamma^\rho [k_1 + k_2, k_2] v_\rho(p_2), \quad (\text{A.33})$$

$$\mathcal{M}_{\bar{\eta}} = -\frac{g_3}{4M_{\text{P}}} f_{abc} \bar{u}(p_1) \gamma^\rho [k_1 + k_2, k_1] v_\rho(p_2). \quad (\text{A.34})$$

The result for the squared amplitudes for the massless case is

$$|\mathcal{M}_\eta|^2 + |\mathcal{M}_{\bar{\eta}}|^2 = -\frac{g_3^2 C_3}{2M_{\text{P}} s} (s + 2t)^2, \quad (\text{A.35})$$

with $|f^{abc}|^2 \rightarrow C_3$. The full amplitude squared for fixed a, b, c is

$$|\mathcal{M}_{A,\text{full}}|^2 = 2 \left(s + 2t + 2\frac{t^2}{s} \right) |f^{abc}|^2 \rightarrow 2C_3 \left(s + 2t + 2\frac{t^2}{s} \right), \quad (\text{A.36})$$

where the factor of $1/2$ (which accounts for the identical incoming gluons) is already included in the result. We also use the fact that $|f^{abc}|^2 \rightarrow C_3$. The amplitudes for $g\tilde{g} \rightarrow g\tilde{G}$ named process B we get from A using (A.24).

• **Amplitudes for $\tilde{q}_i\tilde{g} \rightarrow \tilde{q}_j\tilde{G}$ (process H)**

There are three Feynman diagrams, (1): with a q propagator in the s -channel, (2):

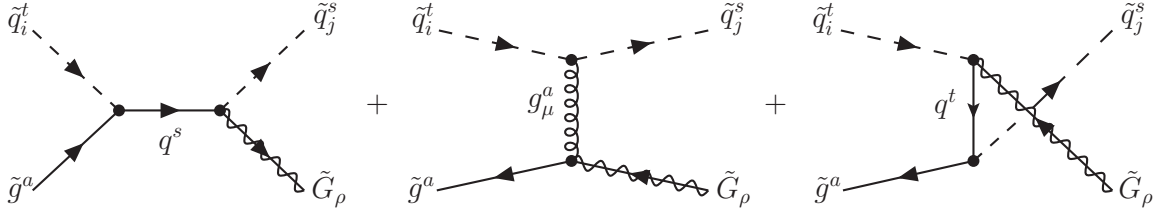


Figure 11. Feynman graphs for the process $\tilde{q}_i\tilde{g} \rightarrow \tilde{q}_j\tilde{G}$.

with a g propagator in the t -channel and (3): a q propagator in the u -channel. Here one has to be careful again because \mathcal{M}_1 gets an additional minus sign due to fermion statistics.

$$\mathcal{M}_1 = -\frac{ig_3}{M_{\text{P}}} \frac{T_{st}^a}{s - m_q^2} \bar{u}_\rho(p_2) \not{p}_1 \gamma^\rho \alpha_{LR}^j (k_1 + k_2 + m_q) \alpha_{RL}^{i*} u(k_2), \quad (\text{A.37})$$

$$\mathcal{M}_2 = \frac{ig_3}{4M_{\text{P}}t} T_{st}^a \bar{v}(k_2) \gamma^\rho [k_1 - \not{p}_1, k_1 + \not{p}_1] v_\rho(p_2) \delta_{ij}, \quad (\text{A.38})$$

$$\mathcal{M}_3 = \frac{ig_3}{M_{\text{P}}} \frac{T_{st}^a}{u - m_q^2} \bar{v}(k_2) \alpha_{LR}^j (k_1 - \not{p}_2 + m_q) \gamma^\rho k_1 \alpha_{RL}^{i*} v_\rho(p_2). \quad (\text{A.39})$$

The full amplitude squared, with fixed color indices and fixed i, j is

$$|\mathcal{M}_{H,\text{full}}|^2 = -2 \left(t + 2s + \frac{s^2}{t} \right) |T_{rs}^a|^2 \delta_{ij} \rightarrow -4C'_3 \left(t + 2s + \frac{s^2}{t} \right). \quad (\text{A.40})$$

Now because we consider 6 squarks–anti-squarks pairs we get a factor of 2, for the two mass eigenstates for each flavour. Thus for this process we get $|T_{rs}^a|^2 \rightarrow 2C'_3$. The amplitudes for $\tilde{q}_i\tilde{q}_j^* \rightarrow \tilde{g}\tilde{G}$ named process J we get from H using (A.24).

• **Amplitudes for $\tilde{q}_i g \rightarrow q\tilde{G}$ (process C)**

There are four Feynman diagrams, (1): with the four-point interaction, (2): with a \tilde{q} propagator in the s -channel and (3): a \tilde{g} propagator in the t -channel, and (4): a q

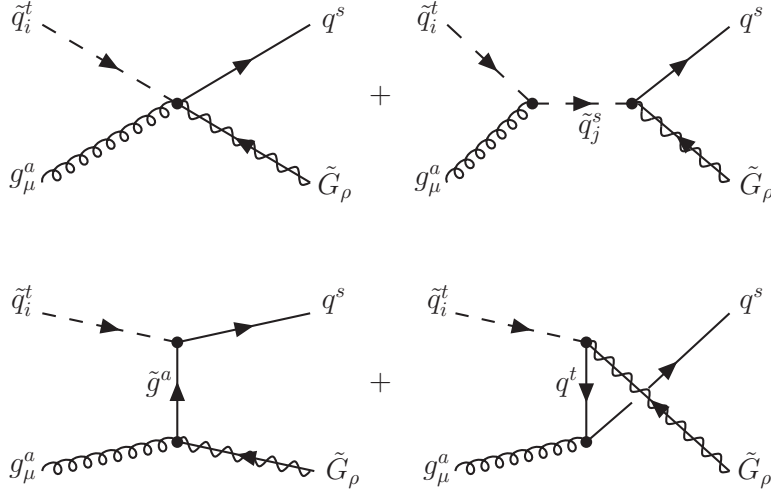


Figure 12. Feynman graphs for the process $\tilde{q}_i g \rightarrow q \tilde{G}$.

propagator in the u -channel,

$$\mathcal{M}_1 = -\frac{ig_3}{\sqrt{2}M_{\text{P}}} T_{st}^a \bar{u}(p_1) \gamma^\rho \gamma^\mu \alpha_{RL}^{i*} v_\rho(p_2) \epsilon_\mu(k_2), \quad (\text{A.41})$$

$$\mathcal{M}_2 = \frac{ig_3}{\sqrt{2}M_{\text{P}}} \frac{T_{st}^a}{s - m_{\tilde{q}_i}^2} \bar{u}(p_1) \gamma^\rho (\not{k}_1 + \not{k}_2) \alpha_{RL}^{i*} v_\rho(p_2) (2k_1 + k_2)^\mu \epsilon_\mu(k_2), \quad (\text{A.42})$$

$$\mathcal{M}_3 = \frac{i\sqrt{2}g_3}{4M_{\text{P}}} \frac{T_{st}^a}{t - M_{N_3}^2} \bar{u}(p_1) \alpha_{RL}^{i*} (\not{k}_1 - \not{p}_1 - m_{\tilde{g}}) \gamma^\rho [\not{k}_2, \gamma^\mu] v_\rho(p_2) \epsilon_\mu(k_2), \quad (\text{A.43})$$

$$\mathcal{M}_4 = \frac{ig_3}{\sqrt{2}M_{\text{P}}} \frac{T_{st}^a}{u - m_q^2} \bar{u}(p_1) \gamma^\mu (\not{k}_1 - \not{p}_2 + m_q) \gamma^\rho \not{k}_1 \alpha_{RL}^{i*} v_\rho(p_2) \epsilon_\mu(k_2). \quad (\text{A.44})$$

The full amplitude squared, with fixed color indices a, r, s and fixed sfermion mass eigenstate indices i, j , is

$$|\mathcal{M}_{C,\text{full}}|^2 = 2s |T_{rs}^a|^2 \delta_{ij} \rightarrow 4s C'_3. \quad (\text{A.45})$$

With 6 squarks and 6 anti-squarks, and $\sum_{a,r,s} |T_{rs}^a|^2 = 4$, along with the sum over i, j yielding 2, this results in a factor of $2C'_3$, where $C'_3 = 4 \times 2 \times 6 = 48$. The amplitudes for $\tilde{q}_i \bar{q} \rightarrow g \tilde{G}$ named process E we get from C using (A.24). The amplitudes for $g \bar{q} \rightarrow \tilde{q}_i^* \tilde{G}$ named process D we get from E using (A.23).

• **Amplitudes for $q \tilde{g} \rightarrow q \tilde{G}$ (process G)**

There are three Feynman diagrams, (1): with a \tilde{q}_i propagator in the s -channel, (2): with a g propagator in the t -channel and (3): a \tilde{q}_i propagator in the u -channel. Here one has to be careful again because \mathcal{M}_3 gets an additional minus sign from fermion

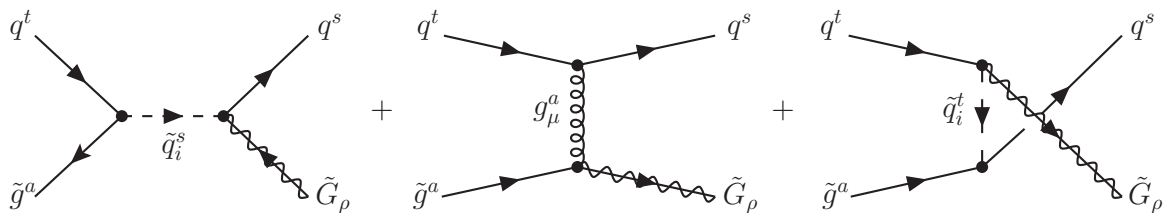


Figure 13. Feynman graphs for the process $q\tilde{g} \rightarrow q\tilde{G}$.

statistics.

$$\mathcal{M}_1 = \sum_{i=1}^2 \frac{ig_3}{M_{\text{P}}} \frac{T_{st}^a}{s - m_{\tilde{q}_i}^2} \bar{v}(k_2) \alpha_{LR}^i u(k_1) \bar{u}(p_1) \gamma^\mu (\not{k}_1 + \not{k}_2) \alpha_{RL}^{i*} v_\mu(p_2), \quad (\text{A.46})$$

$$\mathcal{M}_2 = \frac{ig_3}{4M_{\text{P}}} \frac{T_{st}^a}{t} \bar{u}(p_1) \gamma_\nu u(k_1) \bar{u}_\mu(p_2) [\not{k}_1 - \not{p}_1, \gamma^\nu] \gamma^\mu u(k_2) \quad (\text{A.47})$$

$$\mathcal{M}_3 = \sum_{i=1}^2 \frac{ig_3}{M_{\text{P}}} \frac{T_{st}^a}{u - m_{\tilde{q}_i}^2} \bar{u}(p_1) \alpha_{RL}^{i*} u(k_2) \bar{u}_\mu(p_2) (\not{p}_2 - \not{k}_1) \gamma^\mu \alpha_{LR}^{i*} u(k_1), \quad (\text{A.48})$$

The full amplitude squared, with fixed a, r, s , is

$$|\mathcal{M}_{G,\text{full}}|^2 = -4 \left(s + \frac{s^2}{t} \right) |T_{rs}^a|^2 \rightarrow -8C'_3 \left(s + \frac{s^2}{t} \right). \quad (\text{A.49})$$

Since there are 6 quarks–anti-quarks pairs, we have $|T_{rs}^a|^2 \rightarrow 2C'_3$. The amplitudes for $q\bar{q} \rightarrow g\tilde{G}$ named process I we get from G using (A.24).

The remaining processes can be derived using crossing symmetries, with only potential differences in overall factors. For example, process B does not include the additional factor of $\frac{1}{2}$ that is present in process A. Processes D and E share the same overall factors as process C. Process I, however, involves an incoming quark and antiquark, resulting in a factor 2 less than in process G, where we summed over quarks and antiquarks. A similar reasoning applies to process J in comparison to process H.

A.4 Goldstino production

We have two possibilities to calculate that processes, the so-called derivative and non-derivative approach. The total amplitudes must be the same in both approaches [126].

A.4.1 The derivative approach

According to the equivalence theorem in the derivative approach, the gravitino spinors must be replaced in all amplitudes by goldstino spinors using the following rules:

$$v_\mu(p_2) \rightarrow i\sqrt{\frac{2}{3}} \frac{1}{m_{3/2}} v(p_2) p_{2\mu}, \quad \bar{u}_\mu(p_2) \rightarrow i\sqrt{\frac{2}{3}} \frac{1}{m_{3/2}} \bar{u}(p_2) p_{2\mu}. \quad (\text{A.50})$$

A.4.2 The non-derivative approach

Here one has new Feynman rules, which can be found e.g. in the [7] or in [8]. The goldstino-fermion-sfermion-gluon vertex vanishes and there occurs a new coupling, goldstino-gaugino-sfermion-sfermion. The goldstino-fermion-sfermion coupling is proportional to $m_f^2 - m_{\tilde{f}}^2$. All the other couplings are proportional to the gaugino mass term M_i ($M_3 = m_{\tilde{g}}$). We are only interested in the massless limit. Thus we set the goldstino-fermion-sfermion coupling to zero. We again give only the results for $SU(3)_c$. For convenience we define the prefactor P_f

$$P_f \equiv \frac{m_{\tilde{g}}}{2\sqrt{6}M_{\text{P}}m_{3/2}}g_3(f_{abc}|T_{rs}^a), \quad (\text{A.51})$$

where f_{abc} (T_{rs}^a) is taken in processes without (with) quarks and squarks. In the amplitudes we set all other occurring $m_{\tilde{g}}$ to zero.

For $\tilde{g}\tilde{g} \rightarrow \tilde{g}\tilde{G}$, named process F in table 1 we again have three Feynman diagrams, with a g propagator in the s -channel (1), t -channel (2) and u -channel (3), all connected by crossing symmetries. \mathcal{M}_2 gets an additional minus sign from fermion statistics.

$$\mathcal{M}_1 = i\frac{P_f}{s}\bar{v}(k_2)\gamma_\mu u(k_1)\bar{u}(p_2)[\not{k}_1 + \not{k}_2, \gamma^\mu]v(p_1), \quad (\text{A.52})$$

$$\mathcal{M}_2 = -i\frac{P_f}{t}\bar{u}(p_1)\gamma_\mu u(k_1)\bar{u}(p_2)[\not{p}_1 - \not{k}_1, \gamma^\mu]u(k_2), \quad (\text{A.53})$$

$$\mathcal{M}_3 = i\frac{P_f}{t}\bar{u}(p_1)\gamma_\mu u(k_2)\bar{u}(p_2)[\not{p}_2 - \not{k}_1, \gamma^\mu]u(k_1). \quad (\text{A.54})$$

For $gg \rightarrow \tilde{g}\tilde{G}$, named process A in table 1 we again have four Feynman diagrams, (1): with the four-point interaction, (2): with a g propagator in the s -channel, (3): a \tilde{g} propagator in the t -channel, and (4): a \tilde{g} propagator in the u -channel,

$$\mathcal{M}_1 = iP_f\bar{u}(p_2)[\gamma^\mu, \gamma^\nu]v(p_1)\epsilon_\mu(k_1)\epsilon_\nu(k_2). \quad (\text{A.55})$$

$$\mathcal{M}_2 = -i\frac{P_f}{s}V^{\mu\nu\rho}(k_1, k_2, -k_1 - k_2)\bar{u}(p_2)[\not{k}_1 + \not{k}_2, \gamma_\rho]v(p_1)\epsilon_\mu(k_1)\epsilon_\nu(k_2), \quad (\text{A.56})$$

$$\mathcal{M}_3 = i\frac{P_f}{t}\bar{u}(p_2)[\not{k}_2, \gamma^\nu](\not{k}_1 - \not{p}_1)\gamma^\mu v(p_1)\epsilon_\mu(k_1)\epsilon_\nu(k_2), \quad (\text{A.57})$$

$$\mathcal{M}_4 = -i\frac{P_f}{u}\bar{u}(p_2)[\not{k}_1, \gamma^\mu](\not{k}_2 - \not{p}_1)\gamma^\nu v(p_1)\epsilon_\mu(k_1)\epsilon_\nu(k_2). \quad (\text{A.58})$$

For the $\xi = 1$ gauge we also need the matrix elements with the incoming FP-ghosts of the gluon. There are two graphs possible,

$$\mathcal{M}_\eta = -i\frac{P_f}{s}\bar{u}(p_2)\gamma^\rho[\not{k}_1 + \not{k}_2, \not{k}_2]v(p_1), \quad (\text{A.59})$$

$$\mathcal{M}_{\bar{\eta}} = -i\frac{P_f}{s}\bar{u}(p_2)\gamma^\rho[\not{k}_1 + \not{k}_2, \not{k}_1]v(p_1). \quad (\text{A.60})$$

The result for the squared amplitudes for the massless case is

$$|\mathcal{M}_\eta|^2 + |\mathcal{M}_{\bar{\eta}}|^2 = -4\frac{P_f}{s}C(s + 2t)^2, \quad (\text{A.61})$$

with $C_3 = \sum_{a,b,c} |f^{abc}|^2 = 24$ for $SU(3)_c$.

For $\tilde{q}\tilde{g} \rightarrow \tilde{q}\tilde{G}$, named process H in table 1 we have two graphs, with a g propagator in the t -channel and a new one, with the four-point interaction squark-squark-guino-goldstino,

$$\mathcal{M}_1 = \frac{P_f}{t} \bar{u}(p_2) [\not{k}_1 - \not{p}_1, \not{p}_1 + \not{k}_1] u(k_2), \quad (\text{A.62})$$

$$\mathcal{M}_2 = 2 P_f \bar{u}(p_2) (P_R - P_L) u(k_2), \quad (\text{A.63})$$

with $P_R - P_L = \gamma_5$. Note that the quartic coupling is taken from [8], page 68, and differs from this in [7], page 61.

The conjugated amplitudes read

$$\mathcal{M}_1^* = -\frac{P_f}{t} \bar{u}(k_2) [\not{k}_1 - \not{p}_1, \not{p}_1 + \not{k}_1] u(p_2), \quad (\text{A.64})$$

$$\mathcal{M}_2^* = -2 P_f \bar{u}(k_2) (P_R - P_L) u(p_2), \quad (\text{A.65})$$

For the squared elements we get

$$|\mathcal{M}_1|^2 = -8 \frac{(2s+t)^2}{t} \quad (\text{A.66})$$

$$|\mathcal{M}_2|^2 = -8t \quad (\text{A.67})$$

$$\mathcal{M}_1 \mathcal{M}_2^* = -\mathcal{M}_2 \mathcal{M}_1^* = 32i \epsilon_{\mu\nu\rho\delta} k_1^\mu k_2^\nu p_1^\rho p_2^\delta. \quad (\text{A.68})$$

The results read, including the prefactor and a factor of 2 for the two squark mass eigenstates,

$$|\mathcal{M}_{\text{full}}|^2 = -4C'_3 \left(t + 2s + \frac{2s^2}{t} \right) \frac{g_3^2}{M_{\text{P}}^2} \frac{M_{N_3}^2}{3m_{3/2}^2}, \quad (\text{A.69})$$

$$|\mathcal{M}_{\text{sub}}|^2 = 0. \quad (\text{A.70})$$

For $\tilde{q}_i g \rightarrow q\tilde{G}$, named process C in table 1 we have only one graphs, with a \tilde{g} propagator in the t -channel,

$$\mathcal{M}_1 = iP_f \frac{\sqrt{2}}{t} \bar{u}(p_1) \alpha_{RL}^{i*} (\not{k}_1 - \not{p}_1) [\not{k}_2, \gamma^\mu] v(p_2) \epsilon_\mu(k_2). \quad (\text{A.71})$$

For $qg \rightarrow q\tilde{G}$, named process G in table 1 we have only one graphs, with a g propagator in the t -channel,

$$\mathcal{M}_1 = i \frac{P_f}{t} \bar{u}(p_1) \gamma_\mu u(k_1) \bar{u}(p_2) [\not{k}_1 - \not{p}_1, \gamma^\mu] u(k_2). \quad (\text{A.72})$$

B Thermal spectral functions

For this calculation we have used the real time formalism (RTF) [133, 134], but we have also checked the validity of our results applying the imaginary time formalism. In the RTF the temperature dependent propagators read as

$$\begin{aligned}
 \text{scalar : } \quad \Delta_S(K, T) &= \frac{i}{K^2} + 2\pi\delta(K^2)n_B(K, T), \\
 \text{fermion : } \quad S_F(K, T) &= \frac{iK}{K^2} - K 2\pi\delta(K^2)n_F(K, T), \\
 \text{vector - boson : } \quad \Delta_{\mu\nu}^{ab}(K, T) &= \delta^{ab}g_{\mu\nu} \left(\frac{-i}{K^2} - 2\pi\delta(K^2)n_B(K, T) \right), \\
 \text{ghost : } \quad G^{ab}(K, T) &= \delta^{ab}\Delta_S(K, T),
 \end{aligned} \tag{B.1}$$

where we have assumed massless particles, at the Feynman $\xi = 1$ gauge. In addition, the Fermion/Boson particle densities are given by

$$n_{F/B}(K, T) = (e^{|K_\mu u^\mu|/T} \pm 1)^{-1}, \tag{B.2}$$

where the four-velocity at the plasma rest frame is $u^\mu = (1, 0, 0, 0)$.

B.1 Vector-boson self-energy

The vector-boson self-energy consists of three different contributions, the scalar, the fermion and the vector-boson one.

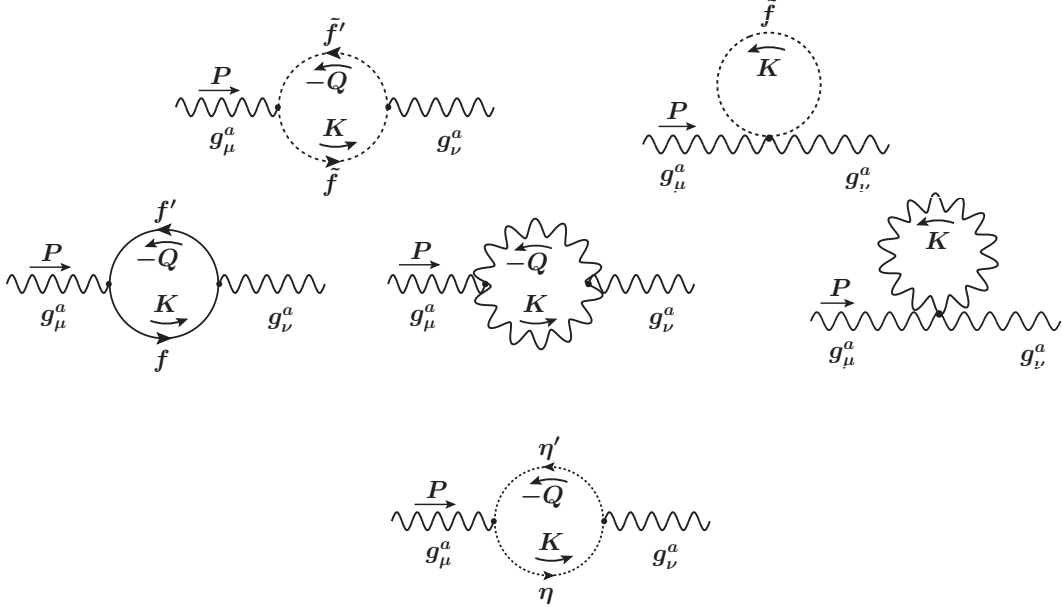


Figure 14. Feynman diagrams for the vector-boson self-energy from the scalar contribution (1st - 2nd), the fermion contribution (3rd) and vector-boson contribution (4th - 6th). The momentum Q is defined as $Q = P - K$.

In figure 14 we display these three different contributions, where the first two diagrams correspond to the scalar one, the third one is the unique diagram with a fermion in the loop and the rest three diagrams are those which are involved in the gauge-boson contribution. Below, we present the real parts of the self-energies $\Pi_{\mu\nu}$ which are needed in our calculation, where the superscripts S, F and V denote the corresponding contributions, that is

$$\begin{aligned}
\text{Re}[\Pi_{\mu\nu}^S(P)] &= -g_N^2 N_S \int \frac{d^4 K}{(2\pi)^3} \left((2K - P)_\mu (2K - P)_\nu - (K - P)^2 g_{\mu\nu} \right) \\
&\quad \times \frac{\delta(K^2)}{(K - P)^2} n_B(K, T), \\
\text{Re}[\Pi_{\mu\nu}^F(P)] &= -4g_N^2 N_F \int \frac{d^4 K}{(2\pi)^3} \left((K - P)_{(\mu} K_{\nu)} + K_\rho P^\rho g_{\mu\nu} \right) \frac{\delta(K^2)}{(K - P)^2} n_F(K, T), \\
\text{Re}[\Pi_{\mu\nu}^V(P)] &= g_N^2 N_V \int \frac{d^4 K}{(2\pi)^3} \left(-4(K - P)_{(\mu} K_{\nu)} - (2P^2 + 4K_\rho P^\rho) g_{\mu\nu} + 2P_\mu P_\nu \right) \\
&\quad \times \frac{\delta(K^2)}{(K - P)^2} n_B(K, T). \tag{B.3}
\end{aligned}$$

The numerical coefficients N_S , N_F and N_V for the MSSM are given in table 2. Following the notation of [17] we define the integrals

$$G_i \equiv g^{\mu\nu} \text{Re}(\Pi_{\mu\nu}^i)/(g_N^2 N_i), \quad \text{and} \quad H_i \equiv u^\mu u^\nu \text{Re}(\Pi_{\mu\nu}^i)/(g_N^2 N_i) \tag{B.4}$$

where the subscript i stands for the three different contributions as discussed previously. After manipulations in agreement with [17] we obtain that

$$\begin{aligned}
G_S &= \int_0^\infty \frac{dk}{2\pi^2} \left[2k - \frac{P^2}{8p} L_- \right] n_B(K, T) = \frac{T^2}{6} - \frac{P^2}{16\pi^2 p} I_1^B, \\
G_F &= \int_0^\infty \frac{dk}{2\pi^2} \left[4k + \frac{P^2}{2p} L_- \right] n_F(K, T) = \frac{T^2}{6} + \frac{P^2}{4\pi^2 p} I_1^F, \\
G_V &= \int_0^\infty \frac{dk}{2\pi^2} \left[4k + \frac{5}{4} \frac{P^2}{p} L_- \right] n_B(K, T) = \frac{T^2}{3} + \frac{5P^2}{8\pi^2 p} I_1^B, \\
H_S &= \int_0^\infty \frac{dk}{2\pi^2} \left[k L + \frac{M}{2p} + \frac{p}{8} L_- \right] n_B(K, T) = \frac{T^2}{12} L + \frac{p}{16\pi^2} \left(1 + \frac{P^2}{p^2} \right) I_1^B \\
&\quad + \frac{1}{4\pi^2 p} I_2^B + \frac{p_0}{4\pi^2 p} I_3^B, \\
H_F &= \int_0^\infty \frac{dk}{2\pi^2} \left[2k L + \frac{M}{p} \right] n_F(K, T) = \frac{T^2}{12} L + \frac{P^2}{8\pi^2 p} I_1^F + \frac{1}{2\pi^2 p} I_2^F + \frac{p_0}{2\pi^2 p} I_3^F, \\
H_V &= \int_0^\infty \frac{dk}{2\pi^2} \left[2k L + \frac{M}{p} - \frac{p}{4} L_- \right] n_B(K, T) = \frac{T^2}{6} L - \frac{p}{8\pi^2} \left(1 - \frac{P^2}{p^2} \right) I_1^B \\
&\quad + \frac{1}{2\pi^2 p} I_2^B + \frac{p_0}{2\pi^2 p} I_3^B,
\end{aligned} \tag{B.5}$$

with

$$L = 1 - \frac{p_0}{p} \ln \left(\frac{p_0 + p}{p_0 - p} \right), \quad L_{\pm}(k) = \ln \left(\frac{2k + p_0 + p}{2k + p_0 - p} \right) \pm \ln \left(\frac{2k - p_0 - p}{2k - p_0 + p} \right),$$

$$M(k) = \left(\frac{p_0^2 - p^2}{4} + k^2 \right) L_-(k) + kp_0 L_+(k). \quad (\text{B.6})$$

The second equalities in (B.5) are obtained using the integrals

$$\int_0^{\infty} \frac{dk}{2\pi^2} k n_{B,F}(k) = \frac{T^2}{12}, \frac{T^2}{24} \quad \text{and} \quad I_{\{1,2,3\}}^{B,F} = \int_0^{\infty} dk \{1, k^2, k\} L_{\{-,-,+\}}(k, p_0, p) n_{B,F}(k). \quad (\text{B.7})$$

These integrals $I_{1,2,3}^{F,B}$ have been used in our numerical analysis for the self-energies and the dispersion relations.

B.2 Fermion self-energy

There are two Feynman diagrams (figure 15) contributing to the fermion selfenergy. One that is due to vector boson loop and another due to Yukawa type fermion loop. The relevant interaction Lagrangian is

$$\mathcal{L} = -g_3 g_{\mu}^a \bar{f}_s \gamma^{\mu} T_{st}^a f_t + \lambda_q \phi \bar{f}_s \Gamma_{st} f_t. \quad (\text{B.8})$$

This yields the Feynman rules for the vertex vector-boson(g_{μ}^a)-fermion(\bar{f}_s)-fermion(f_t) = $-ig_3 T_{st}^a \gamma_{\mu}$ and for the scalar(ϕ)-fermion(\bar{f}_s)-fermion(f_t) = $i\lambda \Gamma_{st}$. Using again the

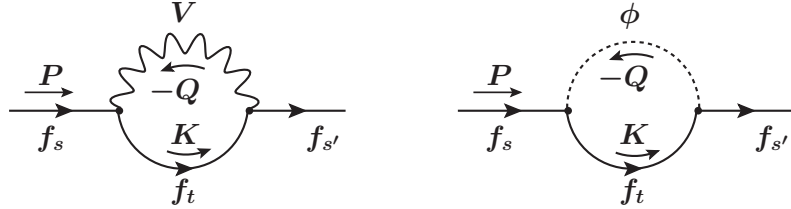


Figure 15. Feynman diagrams for the fermion self-energy from the vector-boson (left) and scalar (right) contribution. The momentum Q is defined as $Q = P - K$.

real time formalism propagators (B.1) we obtain that the real part of the thermally corrected fermion propagator (vector-boson part) is

$$\text{Re}[\Sigma_V(P)] = -2g_3^2 C_R \int \frac{d^4 K}{(2\pi)^3} [K (n_B(K, T) + n_F(K, T)) - \not{P} n_B(K, T)] \frac{\delta(K^2)}{(K - P)^2}, \quad (\text{B.9})$$

where $\Sigma_a T_{s't}^a T_{ts}^a = C_R \delta_{s's}$ is the Casimir operator in the representation R . The scalar part of the fermion self-energy $\text{Re}[\Sigma_{\phi}]$, is the same as (B.9) if we substitute the overall factor $2g_3^2 C_R \rightarrow \lambda_q^2 C'$, where $(\Gamma^{\dagger})_{s's} = C' \delta_{s's}$ [135].

For the $T = 0$ part in each gauge group we have that¹²

$$\Sigma_V^{(0)}(P) = -g_N^2 C_R \not{P} \frac{1}{16\pi^2} \left(2 - r - \ln \frac{-P^2}{\mu^2} - \gamma + \ln 4\pi \right), \quad (\text{B.10})$$

and similarly for $\Sigma_\phi^{(0)}$. Assuming the $\overline{\text{DR}}$ renormalization scheme ($r = 0$) and consequently ignoring the terms $-\gamma + \ln 4\pi$, we obtain the spectral functions for fermion particles (ρ_+) and fermion holes (ρ_-) after some manipulations. These spectral functions, including the $T = 0$ contribution, are given by equation (3.31).

B.3 Dispersion relations

B.3.1 Vector-bosons

The $T \neq 0$ dispersion relation for longitudinal (transverse) modes are given by the poles of the longitudinal (transverse) parts of the vector propagator. For the longitudinal one we have to find the zeros of the equation $p^2(1 - \pi_L/P^2) = 0$ as it is dictated from the longitudinal spectral function (3.28), that is

$$\begin{aligned} p^3 + m_V^2 p \left(1 - \frac{p_0}{p} \ln \frac{p_0 + p}{p_0 - p} \right) + \left(\frac{m_V}{T} \right)^2 \frac{3}{N_1 \pi^2} \left[I_1^B \left(\frac{p_0^2}{4} N_2 - \frac{p^2}{2} N_c \right) \right. \\ \left. + I_2^B N_2 + I_3^B p_0 N_2 + I_1^F \frac{p_0^2 - p^2}{4} N_F + I_2^F N_F + I_3^F p_0 N_F \right] = 0, \end{aligned} \quad (\text{B.11})$$

where the integrals $I_{1,2,3}^{F,B}$ have been defined in (B.7) and the coefficients N_1 and N_2 are the following combinations

$$N_1 = N_V + N_S/2 + N_F/2 \quad \text{and} \quad N_2 = N_V + N_S/2. \quad (\text{B.12})$$

Similarly¹³, the dispersion relation for the transverse modes reads

$$\begin{aligned} p^3 - m_V^2 \frac{p}{2} \left(1 - \frac{p_0}{p} \ln \frac{p_0 + p}{p_0 - p} \right) + m_V^2 \frac{p^3}{p^2 - p_0^2} - \left(\frac{m_V}{T} \right)^2 \frac{3}{2N_1 \pi^2} \left[I_1^B \left(\frac{p_0^2 - p^2}{4} N_2 \right. \right. \\ \left. \left. + p^2 N_c \right) + I_2^B N_2 + I_3^B p_0 N_2 + I_1^F \frac{p_0^2 + p^2}{4} N_F + I_2^F N_F + I_3^F p_0 N_F \right] = 0, \end{aligned} \quad (\text{B.13})$$

B.3.2 Fermions

For the fermionic modes the $T \neq 0$ dispersion relations arise from the poles of the spectral functions (3.31), i.e. when $(p_0 \mp p)/2 + \frac{m_F^2}{T^2} F_\pm = 0$. The 1-loop dispersion

¹²We have used that in $d = 4 - \epsilon$ dimensions $\frac{(2\pi^4)}{i\pi^2} \mu^{4-d} \int \frac{d^d K}{(2\pi)^d} \frac{K}{K^2(P-K)^2} = \frac{i}{16\pi^2} \frac{P}{2} \left(\Delta - \ln \frac{-P^2}{\mu^2} + 2 \right)$ where $\Delta = \frac{2}{\epsilon} - \gamma + \ln 4\pi$ and γ is the Euler-Mascheroni constant.

¹³The HTL limits for the transverse and longitudinal modes are given by the equations $p^3 + 2m_V^2 p - m_V^2 p_0 \ln \frac{p_0 + p}{p_0 - p} = 0$, and $p_0^2 p^3 - p^5 - m_V^2 p p_0^2 - m_V^2 \frac{p_0}{2} (p^2 - p_0^2) \ln \frac{p_0 + p}{p_0 - p} = 0$, respectively. These limits can be found in [133, 134].

relation for both ρ_{\pm} takes the form¹⁴

$$p_0 \mp p - \frac{m_F^2}{2p} \left[\left(1 \mp \frac{p_0}{p} \right) \ln \frac{p_0 + p}{p_0 - p} \pm 2 \right] \\ \mp \left(\frac{m_F}{T} \right)^2 \frac{1}{\pi^2} \frac{p_0 \mp p}{p^2} \left[I_3^B + \frac{p_0 \mp p}{2} I_1^B + I_3^F + \frac{p_0 \pm p}{2} I_1^F \right] = 0. \quad (\text{B.14})$$

C Calculation of the collision term

In this appendix we calculate the collision term for the $2 \rightarrow 2$ interactions following closely the method applied in [8]. Although, as we saw in section 3 only two different collision terms are needed for the calculation of the subtracted rate, we give a table with various results that may be useful in other interactions. All the numerical results shown in this appendix have been calculated and cross checked using various integration routines found in Cuba library [128].

For the process $a + b \rightarrow c + \tilde{G}$ the collision term is given by

$$\mathcal{C} \equiv \gamma = \frac{1}{(2\pi)^8} \int \frac{d^3\mathbf{p}_1}{2E_1} \frac{d^3\mathbf{p}_2}{2E_2} \frac{d^3\mathbf{p}_3}{2E_3} \frac{d^3\mathbf{p}}{2E} \delta^4(P_1 + P_2 - P_3 - P) |\mathcal{M}|^2 f_a f_b (1 \pm f_c). \quad (\text{C.1})$$

Firstly, our aim is to calculate the quantity $\frac{d\mathcal{C}}{d^3p}$, where $d^3\mathbf{p} = d^3p d\Omega_p$. Thus,

$$\frac{d\mathcal{C}}{d^3p} = \frac{1}{2^9 \pi^8 E} \int \frac{d^3\mathbf{p}_1}{2E_1} \frac{d^3\mathbf{p}_2}{2E_2} \frac{d^3\mathbf{p}_3}{2E_3} \int d\Omega_p \delta^4(P_1 + P_2 - P_3 - P) |\mathcal{M}|^2 f_a f_b (1 \pm f_c). \quad (\text{C.2})$$

This calculation will be done in the so-called t -frame, in which the reference momentum is the t -channel momentum $\mathbf{k} = \mathbf{p}_1 - \mathbf{p}_3$. Of course the results are frame independent. Thus we will express the other momenta defining first $\hat{\mathbf{k}} = \hat{\mathbf{z}}$,

$$\mathbf{k} = k(0, 0, 1), \quad \mathbf{p} = E(0, \sin \tilde{\theta}, \cos \tilde{\theta}), \quad \mathbf{p}_3 = E_3(\cos \phi \sin \theta, \sin \phi \sin \theta, \cos \theta). \quad (\text{C.3})$$

In this frame the Mandelstam variables are

$$s = (P_1 + P_2)^2 = (P_3 + P)^2 = 2E E_3(1 - \cos \theta \cos \tilde{\theta} - \sin \theta \sin \tilde{\theta} \sin \phi), \\ t = (P_1 - P_3)^2 = (P - P_2)^2 = (E_1 - E_3)^2 - k^2. \quad (\text{C.4})$$

Before we continue with the computation of (C.2), we will prove some useful identities. We will use the identity

$$\frac{d^3\mathbf{p}_1}{2E_1} = d^4P_1 \delta^4(P_1^2) \Theta(E_1) = dE_1 d^3\mathbf{p}_1 \delta^4(P_1^2) \Theta(E_1), \quad (\text{C.5})$$

and we will insert $\int d^3\mathbf{k} \delta^3(\mathbf{k} - \mathbf{p}_1 + \mathbf{p}_3) = 1$, then

$$\frac{d^3\mathbf{p}_1}{2E_1} = \int d^3\mathbf{k} \delta^3(\mathbf{k} - \mathbf{p}_1 + \mathbf{p}_3) dE_1 d^3\mathbf{p}_1 \delta^4(E_1^2 - |\mathbf{p}_1|^2) \Theta(E_1), \quad (\text{C.6})$$

¹⁴In the HTL approximation the terms contain integrals can be dropped, so (B.14) reduces to $p_0 \mp p - \frac{m_F^2}{2p} \left[\left(1 \mp \frac{p_0}{p} \right) \ln \frac{p_0 + p}{p_0 - p} \pm 2 \right] = 0$, [133, 134].

and after integrating over $d^3\mathbf{p}_1$ using the δ -function we get

$$\frac{d^3\mathbf{p}_1}{2E_1} = \delta(E_1^2 - |\mathbf{k} + \mathbf{p}_3|^2)\Theta(E_1)dE_1d^3\mathbf{k}. \quad (\text{C.7})$$

Another usefull identity is

$$\frac{d^3\mathbf{p}_1}{2E_1} = dE_1d^3\mathbf{p}_1\delta^4(P_1^2)\Theta(E_1) = \frac{\delta(E_1 - |\mathbf{p}_1|)}{2|\mathbf{p}_1|}\Theta(E_1)dE_1d^3\mathbf{p}_1, \quad (\text{C.8})$$

which after multiplying by $\delta^4(P_1 + P_2 - P_3 - P)$ becomes

$$\frac{d^3\mathbf{p}_1}{2E_1} \delta^4(P_1 + P_2 - P_3 - P) = \delta((E_3 + E - E_2)^2 - |\mathbf{k} + \mathbf{p}_3|^2)\Theta(E_3 + E - E_2). \quad (\text{C.9})$$

In this calculation, we will use (C.7) as it is and (C.9) expressed in terms of \mathbf{p}_2 and E_2

$$\frac{d^3\mathbf{p}_2}{2E_2} \delta^4(P_1 + P_2 - P_3 - P) = \delta((E_3 + E - E_1)^2 - |\mathbf{p} - \mathbf{k}|^2)\Theta(E_3 + E - E_1). \quad (\text{C.10})$$

Now, the next step is to rewrite the δ -functions in terms of $\cos\theta$ and $\cos\tilde{\theta}$. We have

$$\begin{aligned} \delta(E_1^2 - |\mathbf{k} + \mathbf{p}_3|^2) &= \frac{1}{2E_3k} \delta\left(\cos\theta - \frac{E_1^2 - E_3^2 - k^2}{2E_3k}\right), \quad (\text{C.11}) \\ \delta((E + E_3 - E_1)^2 - |\mathbf{p} - \mathbf{k}|^2) &= \frac{1}{2Ek} \delta\left(\cos\tilde{\theta} - \frac{E^2 + k^2 - (E + E_3 - E_1)^2}{2Ek}\right). \end{aligned}$$

Substituting (C.7), (C.10), and (C.11) in (C.2) we get

$$\begin{aligned} \frac{d\mathcal{C}}{d^3p} &= \frac{1}{2^{12}\pi^8 E^2} \int d\cos\tilde{\theta} d\tilde{\phi} d\cos\theta d\phi dE_1 dE_3 dk d\Omega_k \\ &\times \delta\left(\cos\theta - \frac{E_1^2 - E_3^2 - k^2}{2E_3k}\right) \delta\left(\cos\tilde{\theta} - \frac{E^2 + k^2 - (E + E_3 - E_1)^2}{2Ek}\right) \quad (\text{C.12}) \\ &\times |\mathcal{M}|^2 f_a f_b (1 \pm f_c) \Theta(E_1) \Theta(E_3) \Theta(E + E_3 - E_1). \end{aligned}$$

Nothing depends on $d\tilde{\phi}$ and $d\Omega_k$, so after these integrations we get an additional $8\pi^2$ factor. After the θ and $\tilde{\theta}$ integrations we have to substitute

$$\cos\theta = \frac{E_1^2 - E_3^2 - k^2}{2E_3k} \quad \text{and} \quad \cos\tilde{\theta} = \frac{E^2 + k^2 - (E + E_3 - E_1)^2}{2Ek}. \quad (\text{C.13})$$

From the integrations over the δ -functions, we find that

$$-1 \leq \cos\theta \leq 1 \Rightarrow \begin{cases} E_3 - E_1 \leq k \leq E_1 + E_3 \\ E_1 - E_3 \leq k, \end{cases} \quad (\text{C.14})$$

$$-1 \leq \cos \tilde{\theta} \leq 1 \Rightarrow \begin{cases} E_1 - E_3 \leq k \leq 2E + E_3 - E_1 \\ E_3 - E_1 \leq k, \end{cases} \quad (\text{C.15})$$

which yield the Θ -functions $\Theta(k - |E_1 - E_3|)$, $\Theta(E_1 + E_3 - k)$ and $\Theta(2E + E_3 - E_1 - k)$. After performing the remaining angular integrations we find that

$$\frac{d\mathcal{C}}{d^3p} = \frac{1}{2^9 \pi^6 E^2} \int dE_1 dE_3 dq d\phi |\mathcal{M}|^2 f_a f_b (1 \pm f_c) \vartheta, \quad (\text{C.16})$$

where ϑ is defined as

$$\begin{aligned} \vartheta = & \Theta(k - |E_1 - E_3|) \Theta(E_1 + E_3 - k) \\ & \times \Theta(2E + E_3 - E_1 - k) \Theta(E + E_3 - E_1) \Theta(E_1) \Theta(E_3), \end{aligned} \quad (\text{C.17})$$

and in $|\mathcal{M}|^2$ we have substituted θ and $\tilde{\theta}$ from (C.13). Using the identities for the Heaviside step function

$$\Theta(E_1 + E_3 - k) = 1 - \Theta(k - E_1 - E_3), \quad (\text{C.18})$$

$$\Theta(k - E_1 - E_3) \Theta(k - |E_1 - E_3|) = \Theta(k - E_1 - E_3), \quad (\text{C.19})$$

and substituting $1 = \Theta(E_1 - E_3) + \Theta(E_3 - E_1)$ in equation (C.17), we obtain

$$\begin{aligned} \vartheta = & \Theta(k - E_1 + E_3) \Theta(2E + E_3 - E_1 - k) \Theta(E + E_3 - E_1) \Theta(E_1 - E_3) \Theta(E_1) \Theta(E_3) \\ & + \Theta(k + E_1 - E_3) \Theta(2E + E_3 - E_1 - k) \Theta(E + E_3 - E_1) \Theta(E_3 - E_1) \Theta(E_1) \Theta(E_3) \\ & - \Theta(k - E_1 - E_3) \Theta(2E + E_3 - E_1 - k) \Theta(E + E_3 - E_1) \Theta(E_1) \Theta(E_3). \end{aligned} \quad (\text{C.20})$$

Note that $\Theta(k - E_1 - E_3) \Theta(2E + E_3 - E_1 - k) \Rightarrow E_1 < E$, so we have to include the corresponding Θ -function. It is obvious that we will need to calculate 3 different integrals because of the 3 different combinations of Θ -functions in (C.20). We have

$$\vartheta = \vartheta_1 + \vartheta_2 + \vartheta_3, \quad (\text{C.21})$$

where

$$\begin{aligned} \vartheta_1 = & \Theta(k - E_1 + E_3) \Theta(2E + E_3 - E_1 - k) \Theta(E + E_3 - E_1) \Theta(E_1 - E_3) \Theta(E_1) \Theta(E_3), \\ \vartheta_2 = & \Theta(k + E_1 - E_3) \Theta(2E + E_3 - E_1 - k) \Theta(E + E_3 - E_1) \Theta(E_3 - E_1) \Theta(E_1) \Theta(E_3), \\ \vartheta_3 = & -\Theta(k - E_1 - E_3) \Theta(2E + E_3 - E_1 - k) \Theta(E + E_3 - E_1) \Theta(E - E_1) \Theta(E_1) \Theta(E_3). \end{aligned} \quad (\text{C.22})$$

After splitting the ϑ into three terms as in (C.21) we can write

$$\frac{d\mathcal{C}^{|\mathcal{M}|^2}}{d^3p} = \sum_A g_A^{|\mathcal{M}|^2}, \quad (\text{C.23})$$

where $|\mathcal{M}|^2 = \{s, t, s^2, t^2, st\}$ and $A = \{1, 2, 3\}$. We have defined

$$g_A^{|\mathcal{M}|^2} = \frac{1}{2^9 \pi^6 E^2} \int_0^\infty dE_3 \int_0^{E+E_3} dE_1 \int dk \int_0^{2\pi} d\phi |\mathcal{M}|^2 f_{abc} \vartheta_A, \quad (\text{C.24})$$

A	k -limits
1	$E_1 - E_3 \leq k \leq 2E + E_3 - E_1$
2	$E_3 - E_1 \leq k \leq 2E + E_3 - E_1$
3	$E_1 + E_3 \leq k \leq 2E + E_3 - E_1$

Table 4. The integration limits for k for the various cases.

$ \mathcal{M} ^2$	BBF	BFB	FFF
s	$0.260 \cdot 10^{-3}$	$0.271 \cdot 10^{-3}$	$0.151 \cdot 10^{-3}$
t	$-0.130 \cdot 10^{-3}$	$-0.133 \cdot 10^{-3}$	$-0.756 \cdot 10^{-4}$
s^2	$0.540 \cdot 10^{-2}$	$0.546 \cdot 10^{-2}$	$0.418 \cdot 10^{-2}$
t^2	$0.180 \cdot 10^{-2}$	$0.181 \cdot 10^{-2}$	$0.140 \cdot 10^{-2}$
st	$-0.270 \cdot 10^{-2}$	$-0.271 \cdot 10^{-2}$	$-0.209 \cdot 10^{-2}$

Table 5. The values of the collision term normalised by $1/T^6$ (for s and t) or $1/T^8$ (for s^2 , t^2 and st), for the possible statistical factors and the five basic squared amplitudes.

and the statistical factor is $f_{abc} = f_a(E_1)f_b(E_2)(1 \pm f_c(E_3))$. The integration limits for the dk integration are dictated by the theta functions in (C.22). As we have mentioned we will calculate five different amplitudes $|\mathcal{M}|^2$ for completeness. These are $|\mathcal{M}|^2 = s, t, s^2, t^2$ and st . Moreover, since we will integrate analytically over k and ϕ , it will be useful to define the function

$$\tilde{g}_A^{|\mathcal{M}|^2}(E, E_1, E_3) = \frac{1}{2\pi} \int dk \int_0^{2\pi} d\phi |\mathcal{M}|^2. \quad (\text{C.25})$$

Thus from (C.24) and (C.25), we obtain that

$$g_A^{|\mathcal{M}|^2} = \frac{1}{2^8 \pi^5 E^2} \int_0^\infty dE_3 \int_0^{E+E_3} dE_1 \tilde{g}_A^{|\mathcal{M}|^2}(E, E_1, E_3) f_{abc} \vartheta_A. \quad (\text{C.26})$$

Using now the limits from the table 4 based on (C.22), we are ready to calculate $\tilde{g}_A^{|\mathcal{M}|^2}(E, E_1, E_3)$. In details we have

- For $|\mathcal{M}|^2 = s$

$$\begin{aligned} \tilde{g}_1^s &= \frac{4}{3} (E - E_1 + E_3)^2 (E + 2E_1 + E_3), \\ \tilde{g}_2^s &= \frac{4}{3} E^2 (E + 3E_3), \\ \tilde{g}_3^s &= \frac{4}{3} (E - E_1) (E^2 + 3E_3(E + E_1) + EE_1 - 2E_1^2). \end{aligned} \quad (\text{C.27})$$

$ \mathcal{M} ^2$	BBF	BFB	FFF
s	$0.295 \cdot 10^{-3} (+14\%)$	$0.221 \cdot 10^{-3} (-18\%)$	$0.166 \cdot 10^{-3} (+10\%)$
t	$-0.148 \cdot 10^{-3} (+14\%)$	$-0.111 \cdot 10^{-3} (-17\%)$	$-0.830 \cdot 10^{-4} (+10\%)$
s^2	$0.574 \cdot 10^{-2} (+6\%)$	$0.502 \cdot 10^{-2} (-8\%)$	$0.440 \cdot 10^{-2} (+5\%)$
t^2	$0.191 \cdot 10^{-2} (+6\%)$	$0.167 \cdot 10^{-2} (-7\%)$	$0.147 \cdot 10^{-2} (+5\%)$
st	$-0.287 \cdot 10^{-2} (+6\%)$	$-0.251 \cdot 10^{-2} (-7\%)$	$-0.220 \cdot 10^{-2} (+5\%)$

Table 6. The \mathcal{C}' collision term normalised by $1/T^6$ (for s and t) or $1/T^8$ (for s^2 , t^2 and st), where the statistical factor f_c has been neglected. The percentages in the parentheses are the deviations from the value of \mathcal{C} , namely $(\mathcal{C}' - \mathcal{C})/\mathcal{C}$ %.

- For $|\mathcal{M}|^2 = t$

$$\begin{aligned}
\tilde{g}_1^t &= -\frac{4}{3}(E - E_1 + E_3)^2(2E + E_1 - E_3), \\
\tilde{g}_2^t &= -\frac{4}{3}E^2(2E - 3E_1 + 3E_3), \\
\tilde{g}_3^t &= -\frac{4}{3}(E - E_1)(3E_3(E + E_1) + (E - E_1)(2E + E_1)).
\end{aligned} \tag{C.28}$$

- For $|\mathcal{M}|^2 = s^2$

$$\begin{aligned}
\tilde{g}_1^{s^2} &= \frac{16}{15}(E - E_1 + E_3)^3(E^2 + 3EE_1 + 2EE_3 + 6E_1^2 + 3E_1E_3 + E_3^2), \\
\tilde{g}_2^{s^2} &= \frac{16}{15}E^3(E^2 + 5EE_3 + 10E_3^2), \\
\tilde{g}_3^{s^2} &= \frac{16}{15}(5E_3(E^4 - 4EE_1^3 + 3E_1^4) + 10E_3^2(E^3 - E_1^3) + (E^2 + 3EE_1 + 6E_1^2)(E - E_1)^3).
\end{aligned} \tag{C.29}$$

- For $|\mathcal{M}|^2 = t^2$

$$\begin{aligned}
\tilde{g}_1^{t^2} &= \frac{16}{15}(6E^2 + 3E(E_1 - E_3) + (E_1 - E_3)^2)(E - E_1 + E_3)^3, \\
\tilde{g}_2^{t^2} &= \frac{16}{15}E^3(6E^2 + 15E(E_3 - E_1) + 10(E_1 - E_3)^2), \\
\tilde{g}_3^{t^2} &= \frac{16}{15}(6E^5 + 15E^4(E_3 - E_1) + 10E^3(E_1 - E_3)^2 - E_1^3(E_1^2 - 5E_1E_3 + 10E_3^2)).
\end{aligned} \tag{C.30}$$

- Finally, for $|\mathcal{M}|^2 = st$

$$\begin{aligned}
\tilde{g}_1^{st} &= -\frac{16}{15}(E - E_1 + E_3)^3(3E^2 + E(4E_1 + E_3) + (E_1 - E_3)(3E_1 + 2E_3)), \\
\tilde{g}_2^{st} &= -\frac{16}{15}E^3(3E^2 - 5E(E_1 - 2E_3) + 10E_3(E_3 - E_1)), \\
\tilde{g}_3^{st} &= -\frac{16}{15}\left[10E_3^2(E^3 - E_1^3) + 10E_3(E^2 + EE_1 + E_1^2)(E - E_1)^2\right. \\
&\quad \left.+ (3E^2 + 4EE_1 + 3E_1^2)(E - E_1)^3\right].
\end{aligned} \tag{C.31}$$

Based on the previous analytical results for the $\tilde{g}_A^{|\mathcal{M}|^2}(E, E_1, E_3)$ we will use the relation

$$\mathcal{C}_{abc}^{|\mathcal{M}|^2} = \frac{1}{2^8 \pi^5} \int_0^\infty dE \int_0^\infty dE_3 \int_0^{E+E_3} dE_1 \sum_A \{ \tilde{g}_A^{|\mathcal{M}|^2}(E, E_1, E_3) \vartheta_A \} f_{abc}, \quad (\text{C.32})$$

in order to perform numerically the integrations over E_1, E_3 and E . The ϑ_A is taken from (C.21) and the statistical factor f_{abc} can be f_{BBF} , f_{BFB} or f_{FFF} . For all these cases the numerical values for the collision terms, normalised by $1/T^6$ or $1/T^8$ are summarized in the table 5. For our calculation of the subtracted rate we need only the numerical factors $\mathcal{C}_{\text{BBF}}^s = 0.25957 \times 10^{-3}$ and $\mathcal{C}_{\text{BFB}}^t = -0.13286 \times 10^{-3}$.

Moreover ignoring the statistical factor for the accompanying particle of the gravitino, that is $1 \pm f_c(E_3) = 1$, we can calculate the collision factor \mathcal{C}' defined as

$$\mathcal{C}' = \frac{1}{(2\pi)^8} \int \frac{d^3 \mathbf{p}_1}{2E_1} \frac{d^3 \mathbf{p}_2}{2E_2} \frac{d^3 \mathbf{p}_3}{2E_3} \frac{d^3 \mathbf{p}}{2E} \delta^4(P_1 + P_2 - P_3 - P) |\mathcal{M}|^2 f_a f_b, \quad (\text{C.33})$$

analytically. The numerical values for \mathcal{C}' along with the deviations from the value of \mathcal{C} are given in table 6.

References

- [1] G. Belanger, F. Boudjema, A. Pukhov, and A. Semenov, *micrOMEGAs: Version 1.3*, *Comput. Phys. Commun.* **174** (2006) 577–604, [[hep-ph/0405253](#)].
- [2] G. Alguero, G. Belanger, F. Boudjema, S. Chakraborti, A. Goudelis, S. Kraml, A. Mjallal, and A. Pukhov, *micrOMEGAs 6.0: N-component dark matter*, *Comput. Phys. Commun.* **299** (2024) 109133, [[arXiv:2312.14894](#)].
- [3] J. Ellis, K. A. Olive, V. C. Spanos, and I. D. Stamou, *The CMSSM survives Planck, the LHC, LUX-ZEPLIN, Fermi-LAT, H.E.S.S. and IceCube*, *Eur. Phys. J. C* **83** (2023), no. 3 246, [[arXiv:2210.16337](#)].
- [4] T. Moroi, *Gravitino production in the early universe and its implications to particle cosmology*, *AIP Conf. Proc.* **805** (2005), no. 1 37–43, [[hep-ph/0509121](#)].
- [5] M. Bolz, W. Buchmuller, and M. Plumacher, *Baryon asymmetry and dark matter*, *Phys. Lett. B* **443** (1998) 209–213, [[hep-ph/9809381](#)].
- [6] M. Bolz, A. Brandenburg, and W. Buchmuller, *Thermal production of gravitinos*, *Nucl. Phys. B* **606** (2001) 518–544, [[hep-ph/0012052](#)]. [Erratum: *Nucl. Phys. B* 790, 336–337 (2008)].
- [7] M. Bolz, *Thermal Production of Gravitinos*. PhD thesis, Hamburg U., 2000.
- [8] J. Pradler, *Electroweak Contributions to Thermal Gravitino Production*, Master’s thesis, Vienna U., 2006.
- [9] J. R. Ellis, J. E. Kim, and D. V. Nanopoulos, *Cosmological Gravitino Regeneration and Decay*, *Phys. Lett. B* **145** (1984) 181–186.
- [10] T. Moroi, H. Murayama, and M. Yamaguchi, *Cosmological constraints on the light stable gravitino*, *Phys. Lett. B* **303** (1993) 289–294.

- [11] M. Kawasaki and T. Moroi, *Gravitino production in the inflationary universe and the effects on big bang nucleosynthesis*, *Prog. Theor. Phys.* **93** (1995) 879–900, [[hep-ph/9403364](#)].
- [12] J. Ellis, D. V. Nanopoulos, K. A. Olive, and S.-J. Rey, *On the thermal regeneration rate for light gravitinos in the early universe*, *Astropart. Phys.* **4** (1996) 371–386, [[hep-ph/9505438](#)].
- [13] E. Braaten and R. D. Pisarski, *Soft Amplitudes in Hot Gauge Theories: A General Analysis*, *Nucl. Phys. B* **337** (1990) 569–634.
- [14] E. Braaten and T. C. Yuan, *Calculation of screening in a hot plasma*, *Phys. Rev. Lett.* **66** (1991) 2183–2186.
- [15] E. Braaten and R. D. Pisarski, *Simple effective Lagrangian for hard thermal loops*, *Phys. Rev. D* **45** (1992), no. 6 1827.
- [16] J. Pradler and F. D. Steffen, *Thermal gravitino production and collider tests of leptogenesis*, *Phys. Rev. D* **75** (2007) 023509, [[hep-ph/0608344](#)].
- [17] V. S. Rychkov and A. Strumia, *Thermal production of gravitinos*, *Phys. Rev. D* **75** (2007) 075011, [[hep-ph/0701104](#)].
- [18] H. Eberl and V. C. Spanos, *Three-body gravitino decays in the MSSM*, *JHEP* **08** (2013) 055, [[arXiv:1305.6934](#)].
- [19] H. Eberl and V. C. Spanos, *GravitinoPack and decays of supersymmetric metastable particles*, *Comput. Phys. Commun.* **202** (2016) 310–325, [[arXiv:1509.09159](#)].
- [20] H. Eberl, I. D. Gialamas, and V. C. Spanos, *Gravitino thermal production revisited*, *Phys. Rev. D* **103** (2021), no. 7 075025, [[arXiv:2010.14621](#)].
- [21] R. Barbieri, P. Creminelli, A. Strumia, and N. Tetradis, *Baryogenesis through leptogenesis*, *Nucl. Phys. B* **575** (2000) 61–77, [[hep-ph/9911315](#)].
- [22] S. Davidson and A. Ibarra, *A Lower bound on the right-handed neutrino mass from leptogenesis*, *Phys. Lett. B* **535** (2002) 25–32, [[hep-ph/0202239](#)].
- [23] G. Giudice, A. Notari, M. Raidal, A. Riotto, and A. Strumia, *Towards a complete theory of thermal leptogenesis in the SM and MSSM*, *Nucl. Phys. B* **685** (2004) 89–149, [[hep-ph/0310123](#)].
- [24] A. Pilaftsis and T. E. Underwood, *Resonant leptogenesis*, *Nucl. Phys. B* **692** (2004) 303–345, [[hep-ph/0309342](#)].
- [25] M. Raidal, A. Strumia, and K. Turzyski, *Low-scale standard supersymmetric leptogenesis*, *Phys. Lett. B* **609** (2005) 351–359, [[hep-ph/0408015](#)]. [Addendum: *Phys.Lett.B* 632, 752–753 (2006)].
- [26] S. Antusch and A. Teixeira, *Towards constraints on the SUSY seesaw from flavour-dependent leptogenesis*, *JCAP* **02** (2007) 024, [[hep-ph/0611232](#)].
- [27] E. Nardi, Y. Nir, E. Roulet, and J. Racker, *The Importance of flavor in leptogenesis*, *JHEP* **01** (2006) 164, [[hep-ph/0601084](#)].
- [28] A. Abada, S. Davidson, A. Ibarra, F.-X. Josse-Michaux, M. Losada, and A. Riotto, *Flavour Matters in Leptogenesis*, *JHEP* **09** (2006) 010, [[hep-ph/0605281](#)].

- [29] J. R. Ellis, A. D. Linde, and D. V. Nanopoulos, *Inflation Can Save the Gravitino*, *Phys. Lett. B* **118** (1982) 59–64.
- [30] D. V. Nanopoulos, K. A. Olive, and M. Srednicki, *After Primordial Inflation*, *Phys. Lett. B* **127** (1983) 30–34.
- [31] R. Kallosh, L. Kofman, A. D. Linde, and A. Van Proeyen, *Gravitino production after inflation*, *Phys. Rev. D* **61** (2000) 103503, [[hep-th/9907124](#)].
- [32] G. Giudice, A. Riotto, and I. Tkachev, *Thermal and nonthermal production of gravitinos in the early universe*, *JHEP* **11** (1999) 036, [[hep-ph/9911302](#)].
- [33] H. P. Nilles, M. Peloso, and L. Sorbo, *Nonthermal production of gravitinos and inflatinos*, *Phys. Rev. Lett.* **87** (2001) 051302, [[hep-ph/0102264](#)].
- [34] M. Kawasaki, F. Takahashi, and T. T. Yanagida, *Gravitino overproduction in inflaton decay*, *Phys. Lett. B* **638** (2006) 8–12, [[hep-ph/0603265](#)].
- [35] M. Endo, M. Kawasaki, F. Takahashi, and T. T. Yanagida, *Inflaton decay through supergravity effects*, *Phys. Lett. B* **642** (2006) 518–524, [[hep-ph/0607170](#)].
- [36] J. Ellis, M. A. G. Garcia, D. V. Nanopoulos, K. A. Olive, and M. Peloso, *Post-Inflationary Gravitino Production Revisited*, *JCAP* **03** (2016) 008, [[arXiv:1512.05701](#)].
- [37] E. Dudas, Y. Mambrini, and K. Olive, *Case for an EeV Gravitino*, *Phys. Rev. Lett.* **119** (2017), no. 5 051801, [[arXiv:1704.03008](#)].
- [38] K. Kaneta, Y. Mambrini, and K. A. Olive, *Radiative production of nonthermal dark matter*, *Phys. Rev. D* **99** (2019), no. 6 063508, [[arXiv:1901.04449](#)].
- [39] K. Kaneta, W. Ke, Y. Mambrini, K. A. Olive, and S. Verner, *Gravitational production of spin-3/2 particles during reheating*, *Phys. Rev. D* **108** (2023), no. 11 115027, [[arXiv:2309.15146](#)].
- [40] S. Weinberg, *Cosmological Constraints on the Scale of Supersymmetry Breaking*, *Phys. Rev. Lett.* **48** (1982) 1303.
- [41] M. Khlopov and A. D. Linde, *Is it easy to save the gravitino?*, *Phys. Lett. B* **138** (1984) 265–268.
- [42] T. Moroi, *Effects of the gravitino on the inflationary universe*. Phd thesis, 1995. [[hep-ph/9503210](#)].
- [43] F. D. Steffen, *Gravitino dark matter and cosmological constraints*, *JCAP* **09** (2006) 001, [[hep-ph/0605306](#)].
- [44] J. Pradler and F. D. Steffen, *Constraints on the Reheating Temperature in Gravitino Dark Matter Scenarios*, *Phys. Lett. B* **648** (2007) 224–235, [[hep-ph/0612291](#)].
- [45] M. Kawasaki, K. Kohri, T. Moroi, and A. Yotsuyanagi, *Big-Bang Nucleosynthesis and Gravitino*, *Phys. Rev. D* **78** (2008) 065011, [[arXiv:0804.3745](#)].
- [46] M. Kawasaki, K. Kohri, T. Moroi, and Y. Takaesu, *Revisiting big-bang nucleosynthesis constraints on long-lived decaying particles*, *Phys. Rev. D* **97** (2018), no. 2 023502, [[arXiv:1709.01211](#)].

- [47] R. H. Cyburt, J. R. Ellis, B. D. Fields, K. A. Olive, and V. C. Spanos, *Bound-State Effects on Light-Element Abundances in Gravitino Dark Matter Scenarios*, *JCAP* **11** (2006) 014, [[astro-ph/0608562](#)].
- [48] R. H. Cyburt, J. Ellis, B. D. Fields, F. Luo, K. A. Olive, and V. C. Spanos, *Metastable Charged Sparticles and the Cosmological Li7 Problem*, *JCAP* **12** (2012) 037, [[arXiv:1209.1347](#)].
- [49] G. F. Giudice and R. Rattazzi, *Theories with gauge mediated supersymmetry breaking*, *Phys. Rept.* **322** (1999) 419–499, [[hep-ph/9801271](#)].
- [50] K. Choi, K. Hwang, H. B. Kim, and T. Lee, *Cosmological gravitino production in gauge mediated supersymmetry breaking models*, *Phys. Lett. B* **467** (1999) 211–217, [[hep-ph/9902291](#)].
- [51] T. Asaka, K. Hamaguchi, and K. Suzuki, *Cosmological gravitino problem in gauge mediated supersymmetry breaking models*, *Phys. Lett. B* **490** (2000) 136–146, [[hep-ph/0005136](#)].
- [52] K. Jedamzik, M. Lemoine, and G. Moulta, *Gravitino dark matter in gauge mediated supersymmetry breaking*, *Phys. Rev. D* **73** (2006) 043514, [[hep-ph/0506129](#)].
- [53] H. Fukushima and R. Kitano, *Gravitino thermal production revisited and a new cosmological scenario of gauge mediation*, *JHEP* **01** (2014) 081, [[arXiv:1311.6228](#)].
- [54] R. G. Leigh and R. Rattazzi, *Supersymmetry, finite temperature and gravitino production in the early universe*, *Phys. Lett. B* **352** (1995) 20–28, [[hep-ph/9503402](#)].
- [55] H. Fujisaki, K. Kumekawa, M. Yamaguchi, and M. Yoshimura, *Particle production and gravitino abundance after inflation*, *Phys. Rev. D* **54** (1996) 2494–2503, [[hep-ph/9511381](#)].
- [56] M. Hashimoto, K. Izawa, M. Yamaguchi, and T. Yanagida, *Gravitino overproduction through moduli decay*, *Prog. Theor. Phys.* **100** (1998) 395–398, [[hep-ph/9804411](#)].
- [57] M. Lemoine, *Gravitational production of gravitinos*, *Phys. Rev. D* **60** (1999) 103522, [[hep-ph/9908333](#)].
- [58] A. L. Maroto and J. R. Pelaez, *The equivalence theorem and the production of gravitinos after inflation*, *Phys. Rev. D* **62** (2000) 023518, [[hep-ph/9912212](#)].
- [59] D. H. Lyth, *The gravitino abundance in supersymmetric 'new' inflation models*, *Phys. Lett. B* **488** (2000) 417–422, [[hep-ph/9911257](#)].
- [60] F. Takayama and M. Yamaguchi, *Gravitino dark matter without r-parity*, *Phys. Lett. B* **485** (2000) 388–392, [[hep-ph/0005214](#)].
- [61] J. L. Feng, A. Rajaraman, and F. Takayama, *Superweakly interacting massive particles*, *Phys. Rev. Lett.* **91** (2003) 011302, [[hep-ph/0302215](#)].
- [62] J. L. Feng, A. Rajaraman, and F. Takayama, *Superwimp dark matter signals from the early universe*, *Phys. Rev. D* **68** (2003) 063504, [[hep-ph/0306024](#)].
- [63] J. R. Ellis, K. A. Olive, Y. Santoso, and V. C. Spanos, *Gravitino dark matter in the CMSSM*, *Phys. Lett. B* **588** (2004) 7–16, [[hep-ph/0312262](#)].
- [64] K. Kohri, M. Yamaguchi, and J. Yokoyama, *Production and dilution of gravitinos by modulus decay*, *Phys. Rev. D* **70** (2004) 043522, [[hep-ph/0403043](#)].

- [65] E. J. Copeland and O. Seto, *Reheating and gravitino production in braneworld inflation*, *Phys. Rev. D* **72** (2005) 023506, [[hep-ph/0505149](#)].
- [66] R. Allahverdi, A. Jokinen, and A. Mazumdar, *Gravitino production from reheating in split supersymmetry*, *Phys. Rev. D* **71** (2005) 043505, [[hep-ph/0410169](#)].
- [67] J. R. Ellis, A. R. Raklev, and O. K. Oye, *Gravitino dark matter scenarios with massive metastable charged particles at the LHC*, *JHEP* **10** (2006) 061, [[hep-ph/0607261](#)].
- [68] M. Y. Khlopov, A. Barrau, and J. Grain, *Gravitino production by primordial black hole evaporation and constraints on the inhomogeneity of the early universe*, *Class. Quant. Grav.* **23** (2006) 1875–1882, [[astro-ph/0406621](#)].
- [69] M. Kawasaki, F. Takahashi, and T. T. Yanagida, *The Gravitino-overproduction problem in inflationary universe*, *Phys. Rev. D* **74** (2006) 043519, [[hep-ph/0605297](#)].
- [70] T. Asaka, S. Nakamura, and M. Yamaguchi, *Gravitinos from heavy scalar decay*, *Phys. Rev. D* **74** (2006) 023520, [[hep-ph/0604132](#)].
- [71] D. G. Cerdeno, K.-Y. Choi, K. Jedamzik, L. Roszkowski, and R. Ruiz de Austri, *Gravitino dark matter in the CMSSM with improved constraints from BBN*, *JCAP* **06** (2006) 005, [[hep-ph/0509275](#)].
- [72] W. Buchmuller, A. Ibarra, T. Shindou, F. Takayama, and D. Tran, *Probing Gravitino Dark Matter with PAMELA and Fermi*, *JCAP* **09** (2009) 021, [[arXiv:0906.1187](#)].
- [73] R. H. Cyburt, J. Ellis, B. D. Fields, F. Luo, K. A. Olive, and V. C. Spanos, *Nucleosynthesis Constraints on a Massive Gravitino in Neutralino Dark Matter Scenarios*, *JCAP* **10** (2009) 021, [[arXiv:0907.5003](#)].
- [74] R. H. Cyburt, J. Ellis, B. D. Fields, F. Luo, K. A. Olive, and V. C. Spanos, *Nuclear Reaction Uncertainties, Massive Gravitino Decays and the Cosmological Lithium Problem*, *JCAP* **10** (2010) 032, [[arXiv:1007.4173](#)].
- [75] J. L. Feng, M. Kamionkowski, and S. K. Lee, *Light gravitinos at colliders and implications for cosmology*, *Phys. Rev. D* **82** (2010) 015012, [[arXiv:1004.4213](#)].
- [76] C. Cheung, G. Elor, and L. Hall, *Gravitino freeze-in*, *Phys. Rev. D* **84** (2011) 115021, [[arXiv:1103.4394](#)].
- [77] I. Dalianis, *R-Symmetry and Gravitino Abundance*, *Phys. Rev. D* **85** (2012) 061301, [[arXiv:1110.2072](#)].
- [78] I. Dalianis, *Gravitino dark matter production at finite temperature*, *JHEP* **11** (2013) 162, [[arXiv:1304.7673](#)].
- [79] M. Badziak, I. Dalianis, and Z. Lalak, *Suppressing gravitino thermal production with a temperature-dependent messenger coupling*, *JHEP* **02** (2016) 173, [[arXiv:1512.06795](#)].
- [80] S. Antusch and K. Dutta, *Non-thermal Gravitino Production in Tribid Inflation*, *Phys. Rev. D* **92** (2015) 083503, [[arXiv:1505.04022](#)].
- [81] Y. Ema, K. Mukaida, K. Nakayama, and T. Terada, *Nonthermal gravitino production after large field inflation*, *JHEP* **11** (2016) 184, [[arXiv:1609.04716](#)].

- [82] R. Arya, N. Mahajan, and R. Rangarajan, *Gravitino production in a thermal Universe revisited*, *Phys. Lett. B* **772** (2017) 258–264, [[arXiv:1608.03386](#)].
- [83] K. Nakayama, F. Takahashi, and T. T. Yanagida, *Gravitino problem in supergravity chaotic inflation and susy breaking scale after bicep2*, *Phys. Lett. B* **734** (2014) 358–363, [[arXiv:1404.2472](#)].
- [84] M. A. G. Garcia, Y. Mambrini, K. A. Olive, and M. Peloso, *Enhancement of the Dark Matter Abundance Before Reheating: Applications to Gravitino Dark Matter*, *Phys. Rev. D* **96** (2017), no. 10 103510, [[arXiv:1709.01549](#)].
- [85] K. Benakli, Y. Chen, E. Dudas, and Y. Mambrini, *Minimal model of gravitino dark matter*, *Phys. Rev. D* **95** (2017), no. 9 095002, [[arXiv:1701.06574](#)].
- [86] R. T. Co, F. D’Eramo, and L. J. Hall, *Gravitino or axino dark matter with reheat temperature as high as 10^{16} gev*, *JHEP* **03** (2017) 005, [[arXiv:1611.05028](#)].
- [87] M. A. G. Garcia and M. A. Amin, *Prethermalization production of dark matter*, *Phys. Rev. D* **98** (2018), no. 10 103504, [[arXiv:1806.01865](#)].
- [88] E. Dudas, T. Gherghetta, K. Kaneta, Y. Mambrini, and K. A. Olive, *Gravitino decay in high scale supersymmetry with R -parity violation*, *Phys. Rev. D* **98** (2018), no. 1 015030, [[arXiv:1805.07342](#)].
- [89] J. Ellis, M. A. G. Garcia, N. Nagata, D. V. Nanopoulos, and K. A. Olive, *Superstring-inspired particle cosmology: Inflation, neutrino masses, leptogenesis, dark matter & the susy scale*, *JCAP* **01** (2020) 035, [[arXiv:1910.11755](#)].
- [90] Y. Gu, M. Khlopov, L. Wu, J. M. Yang, and B. Zhu, *Light gravitino dark matter: LHC searches and the Hubble tension*, *Phys. Rev. D* **102** (2020), no. 11 115005, [[arXiv:2006.09906](#)].
- [91] S. Kawai and N. Okada, *Gravitino constraints on supergravity inflation*, *Phys. Rev. D* **105** (2022), no. 10 L101302, [[arXiv:2111.03645](#)].
- [92] W. Ahmed, A. Karozas, and G. K. Leontaris, *Gravitino dark matter, nonthermal leptogenesis, and low reheating temperature in no-scale Higgs inflation*, *Phys. Rev. D* **104** (2021), no. 5 055025, [[arXiv:2104.04328](#)].
- [93] G. Choi and T. T. Yanagida, *Gravitino cosmology helped by a right handed (s)neutrino*, *Phys. Lett. B* **827** (2022) 136954, [[arXiv:2104.02958](#)].
- [94] A. Afzal, W. Ahmed, M. U. Rehman, and Q. Shafi, *μ -hybrid inflation, gravitino dark matter, and stochastic gravitational wave background from cosmic strings*, *Phys. Rev. D* **105** (2022), no. 10 103539, [[arXiv:2202.07386](#)].
- [95] W. Ahmed, M. Junaid, S. Nasri, and U. Zubair, *Constraining the cosmic strings gravitational wave spectra in no-scale inflation with viable gravitino dark matter and nonthermal leptogenesis*, *Phys. Rev. D* **105** (2022), no. 11 115008, [[arXiv:2202.06216](#)].
- [96] M. Deshpande, J. Hamann, D. Sengupta, M. White, A. G. Williams, and Y. Y. Y. Wong, *Revisiting cosmological constraints on supersymmetric SuperWIMPs*, *Eur. Phys. J. C* **84** (2024), no. 7 667, [[arXiv:2309.05709](#)].
- [97] W. Deng, L. Guo, C. Han, and Z. Lei, *Probing Non-Thermal Gravitinos Through Large-Scale Structure Observations*, [arXiv:2408.10585](#).

- [98] F. Hasegawa, K. Mukaida, K. Nakayama, T. Terada, and Y. Yamada, *Gravitino Problem in Minimal Supergravity Inflation*, *Phys. Lett. B* **767** (2017) 392–397, [[arXiv:1701.03106](#)].
- [99] E. W. Kolb, A. J. Long, and E. McDonough, *Catastrophic production of slow gravitinos*, *Phys. Rev. D* **104** (2021), no. 7 075015, [[arXiv:2102.10113](#)].
- [100] E. W. Kolb, A. J. Long, and E. McDonough, *Gravitino Swampland Conjecture*, *Phys. Rev. Lett.* **127** (2021), no. 13 131603, [[arXiv:2103.10437](#)].
- [101] E. Dudas, M. A. G. Garcia, Y. Mambrini, K. A. Olive, M. Peloso, and S. Verner, *Slow and Safe Gravitinos*, *Phys. Rev. D* **103** (2021) 123519, [[arXiv:2104.03749](#)].
- [102] T. Terada, *Minimal supergravity inflation without slow gravitino*, *Phys. Rev. D* **103** (2021), no. 12 125022, [[arXiv:2104.05731](#)].
- [103] I. Antoniadis, K. Benakli, and W. Ke, *Salvage of too slow gravitinos*, *JHEP* **11** (2021) 063, [[arXiv:2105.03784](#)].
- [104] N. Cribiori, D. Lust, and M. Scalisi, *The gravitino and the swampland*, *JHEP* **06** (2021) 071, [[arXiv:2104.08288](#)].
- [105] A. Castellano, A. Font, A. Herraez, and L. E. Ibáñez, *A gravitino distance conjecture*, *JHEP* **08** (2021) 092, [[arXiv:2104.10181](#)].
- [106] M. A. Garcia, Y. Mambrini, K. A. Olive, and S. Verner, *Case for decaying spin-3/2 dark matter*, *Phys. Rev. D* **102** (2020), no. 8 083533, [[arXiv:2006.03325](#)].
- [107] J. C. Criado, N. Koivunen, M. Raidal, and H. Veermäe, *Dark matter of any spin – an effective field theory and applications*, *Phys. Rev. D* **102** (2020), no. 12 125031, [[arXiv:2010.02224](#)].
- [108] J. C. Criado, A. Djouadi, N. Koivunen, M. Raidal, and H. Veermäe, *Higher-spin particles at high-energy colliders*, *JHEP* **05** (2021) 254, [[arXiv:2102.13652](#)].
- [109] G. Casagrande, E. Dudas, and M. Peloso, *On energy and particle production in cosmology: the particular case of the gravitino*, *JHEP* **06** (2024) 003, [[arXiv:2310.14964](#)].
- [110] M. Cirelli, A. Strumia, and J. Zupan, *Dark Matter*, [[arXiv:2406.01705](#)].
- [111] J. C. Criado, A. Djouadi, N. Koivunen, K. Mürsepp, M. Raidal, and H. Veermäe, *Confronting spin-3/2 and other new fermions with the muon $g-2$ measurement*, *Phys. Lett. B* **820** (2021) 136491, [[arXiv:2104.03231](#)].
- [112] M. Kawasaki, A. Kusenko, Y. Tada, and T. T. Yanagida, *Primordial black holes as dark matter in supergravity inflation models*, *Phys. Rev. D* **94** (2016), no. 8 083523, [[arXiv:1606.07631](#)].
- [113] T.-J. Gao and Z.-K. Guo, *Primordial Black Hole Production in Inflationary Models of Supergravity with a Single Chiral Superfield*, *Phys. Rev. D* **98** (2018), no. 6 063526, [[arXiv:1806.09320](#)].
- [114] Y. Aldabergenov, A. Addazi, and S. V. Ketov, *Primordial black holes from modified supergravity*, *Eur. Phys. J. C* **80** (2020), no. 10 917, [[arXiv:2006.16641](#)].
- [115] D. V. Nanopoulos, V. C. Spanos, and I. D. Stamou, *Primordial Black Holes from No-Scale Supergravity*, *Phys. Rev. D* **102** (2020), no. 8 083536, [[arXiv:2008.01457](#)].

- [116] L. Wu, Y. Gong, and T. Li, *Primordial black holes and secondary gravitational waves from string inspired general no-scale supergravity*, *Phys. Rev. D* **104** (2021), no. 12 123544, [[arXiv:2105.07694](#)].
- [117] V. C. Spanos and I. D. Stamou, *Gravitational waves and primordial black holes from supersymmetric hybrid inflation*, *Phys. Rev. D* **104** (2021), no. 12 123537, [[arXiv:2108.05671](#)].
- [118] I. D. Stamou, *Large curvature fluctuations from no-scale supergravity with a spectator field*, *Phys. Lett. B* **855** (2024) 138798, [[arXiv:2404.02295](#)].
- [119] K. Kohri, T. Moroi, and A. Yotsuyanagi, *Big-bang nucleosynthesis with unstable gravitino and upper bound on the reheating temperature*, *Phys. Rev. D* **73** (2006) 123511, [[hep-ph/0507245](#)].
- [120] J. R. Ellis, D. V. Nanopoulos, and S. Sarkar, *The Cosmology of Decaying Gravitinos*, *Nucl. Phys. B* **259** (1985) 175–188.
- [121] A. Strumia, *Thermal production of axino Dark Matter*, *JHEP* **06** (2010) 036, [[arXiv:1003.5847](#)].
- [122] A. Salvio, A. Strumia, and W. Xue, *Thermal axion production*, *JCAP* **01** (2014) 011, [[arXiv:1310.6982](#)].
- [123] K. Bouzoud and J. Ghiglieri, *Thermal axion production at hard and soft momenta*, [[arXiv:2404.06113](#)].
- [124] R. Casalbuoni, S. De Curtis, D. Dominici, F. Feruglio, and R. Gatto, *A GRAVITINO - GOLDSTINO HIGH-ENERGY EQUIVALENCE THEOREM*, *Phys. Lett. B* **215** (1988) 313–316.
- [125] R. Casalbuoni, S. De Curtis, D. Dominici, F. Feruglio, and R. Gatto, *High-Energy Equivalence Theorem in Spontaneously Broken Supergravity*, *Phys. Rev. D* **39** (1989) 2281.
- [126] T. Lee and G.-H. Wu, *Interactions of a single goldstino*, *Phys. Lett. B* **447** (1999) 83–88, [[hep-ph/9805512](#)].
- [127] J. Wess and J. Bagger, *Supersymmetry and supergravity*. Princeton University Press, Princeton, NJ, USA, 1992.
- [128] T. Hahn, *CUBA: A Library for multidimensional numerical integration*, *Comput. Phys. Commun.* **168** (2005) 78–95, [[hep-ph/0404043](#)].
- [129] P. Fayet, *Spontaneously Broken Supersymmetric Theories of Weak, Electromagnetic and Strong Interactions*, *Phys. Lett. B* **69** (1977) 489.
- [130] P. Fayet, *Mixing Between Gravitational and Weak Interactions Through the Massive Gravitino*, *Phys. Lett. B* **70** (1977) 461.
- [131] P. Fayet, *Weak Interactions of a Light Gravitino: A Lower Limit on the Gravitino Mass from the Decay $\psi \rightarrow \text{Gravitino anti-Photino}$* , *Phys. Lett. B* **84** (1979) 421–426.
- [132] P. Fayet, *Scattering Cross-Sections of the Photino and the Goldstino (Gravitino) on Matter*, *Phys. Lett. B* **86** (1979) 272–278.

- [133] M. L. Bellac, *Thermal Field Theory*. Cambridge Monographs on Mathematical Physics. Cambridge University Press, 2011.
- [134] J. Kapusta and C. Gale, *Finite-temperature field theory: Principles and applications*. Cambridge Monographs on Mathematical Physics. Cambridge University Press, 2011.
- [135] H. Weldon, *Effective Fermion Masses of Order gT in High Temperature Gauge Theories with Exact Chiral Invariance*, *Phys. Rev. D* **26** (1982) 2789.
- [136] H. Weldon, *Covariant Calculations at Finite Temperature: The Relativistic Plasma*, *Phys. Rev. D* **26** (1982) 1394.
- [137] H. Weldon, *Dynamical Holes in the Quark - Gluon Plasma*, *Phys. Rev. D* **40** (1989) 2410.
- [138] H. Weldon, *Structure of the gluon propagator at finite temperature*, *Annals Phys.* **271** (1999) 141–156, [[hep-ph/9701279](#)].
- [139] A. Peshier, K. Schertler, and M. H. Thoma, *One loop selfenergies at finite temperature*, *Annals Phys.* **266** (1998) 162–177, [[hep-ph/9708434](#)].
- [140] H. Weldon, *Structure of the quark propagator at high temperature*, *Phys. Rev. D* **61** (2000) 036003, [[hep-ph/9908204](#)].
- [141] S. P. Martin, *A Supersymmetry primer*, *Adv. Ser. Direct. High Energy Phys.* **18** (1998) 1–98, [[hep-ph/9709356](#)].
- [142] **Planck** Collaboration, N. Aghanim et al., *Planck 2018 results. VI. Cosmological parameters*, [arXiv:1807.06209](#).
- [143] **ATLAS** Collaboration, M. Aaboud et al., *Search for supersymmetry in final states with missing transverse momentum and multiple b -jets in proton-proton collisions at $\sqrt{s} = 13$ TeV with the ATLAS detector*, *JHEP* **06** (2018) 107, [[arXiv:1711.01901](#)].
- [144] **CMS** Collaboration, T. C. Collaboration et al., *Search for supersymmetry in proton-proton collisions at 13 TeV in final states with jets and missing transverse momentum*, *JHEP* **10** (2019) 244, [[arXiv:1908.04722](#)].
- [145] J. Ellis, K. A. Olive, and V. C. Spanos, *Non-universal SUSY models, $g_\mu - 2$, m_H and dark matter*, [arXiv:2407.08679](#).